Performance modeling of single-phase brazed plate heat exchangers

Kim Högnabba

M.Sc. Thesis in Chemical Engineering

Supervisor: Professor Ron Zevenhoven
Laboratory of Process and Systems Engineering
Faculty of Science and Engineering
Åbo Akademi University
November 2021

Abstract

The design of heat exchangers for specific applications entails a number of different calculations in order to determine the appropriate dimensions and characteristics for the heat exchanger unit. The relevant equations can be convoluted and often need to be solved in an iterative fashion. Not only is this time-consuming work, but it can also be prone to human errors if performed by hand. A large number of equations for plate heat exchangers have been proposed in the scientific literature, all with different constraints, from which it can be concluded that no commonly accepted method of calculating heat transfer in plate heat exchangers exists.

The purpose of this work is to develop a software application to assist Loval Oy with the dimensioning aspect of designing specifically brazed plate heat exchangers. It will accomplish this by providing a graphical user interface where the user can input information regarding the fluid streams for a specific application, and in return receive an estimate of the heat exchanger unit dimensions necessary. Additionally, experimental data regarding the heat transfer effectiveness will be collected for a number of heat exchanger designs. The data will be used to construct equations that work specifically for the heat exchangers in question in order to ensure that the software application can produce reliable results.

Preface and Acknowledgements

This thesis has been written in collaboration with the research and development department at Loval Oy and the Laboratory of Process and Systems Engineering at Åbo Akademi.

I want to thank the people at Loval for giving me the opportunity to carry out this interesting, and at times challenging project. I would also like to thank the R&D department headed by Johnny Bäcklund for always providing support when I requested it, and for providing the opportunity to gather experimental data in their laboratory. Lastly, I want to thank my supervisor, Professor Ron Zevenhoven, for suggesting this thesis topic and for providing support during the writing process, and associate professor Frank Pettersson for valuable comments.

Abbreviations, variables, and parameters

A	heat transfer area, m^2
A_c	cross-sectional area, m^2
A_p	heat transfer area per plate, m^2
c_f	correction factor
c_p	specific heat capacity, kJ/kgK
$d_{h,\ sine}$	hydraulic diameter for a sine duct, m
D_h	hydraulic diameter, m
D_P	port diameter, m
F_h	antiderivative of f_h
f	Fanning friction factor
f_D	Darcy friction factor
f_h	function
g	gravitational constant, 9.81 m/s^2
h	enthalpy, kJ/kg
k	thermal conductivity, W/mK
$K(\infty)$	Incremental pressure drop number
$K_d(\infty)$	kinetic energy correction factor
$K_e(\infty)$	momentum flux correction factor
L_H	plate heat transfer length, m
$\dot{m}$	mass flow, kg/s
n_c	number of channels

n_p	number of plates
Nu	Nusselt number
P	Power, W
P_p	wetted perimeter, m
p	pressure, Pa
Pr	Prandtl number
$\dot{Q}$	heat flow, W
R	thermal resistance, K/W
R^2	Coefficient of determination
Re	Reynold number
T	temperature, K or °C
T_m	logarithmic temperature, K
U	overall heat transfer coefficient, W/m^{2}K
u	velocity, m/s
$\dot{V}$	Volume flow, m^3/s
v	kinematic viscosity, m^2/s
W	plate width, m
Λ	chevron wavelength, m
$2a$	chevron wave height, m
α	convective heat transfer coefficient, W/m^{2}K
β	chevron corrugation angle, radians
δ_P	plate thickness, m
η	efficiency

μ	dynamic viscosity, kg/ms
ρ	density, kg/m^3
τ	shear stress, Pa
Φ	surface enlargement factor

Table of Contents

1 Introduction

1.1 Introduction to heat exchangers

Heat exchangers play a central role in many modern technical industries and can be found in a wide variety of applications. In its simplest form, a heat exchanger transfers thermal energy from one set of fluids to another. In a majority of cases, these fluids are separated from one another by a solid wall to prevent mixing, and heat is allowed to be transferred through the surface wall by conduction (Sekulić and Shah, 2003, pp. 1–3). The operating principle is illustrated in Figure 1.1, where heat $\dot{Q}$ is transferred from mass flow $\dot{m}_b$ with enthalpy h_{b1} to mass flow $\dot{m}_a$ with enthalpy h_{a1} in a co-current configuration.

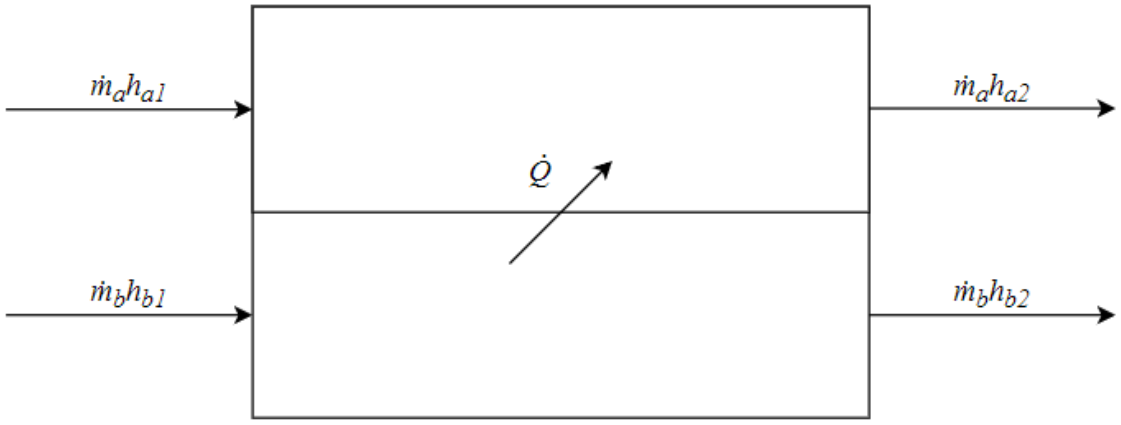

Figure 1.1. Operating principle of a heat exchanger, where $h_{b1} > h_{a1}$.

A wide variety of heat exchanger models and designs exist in the industry today, including shell and tube designs, double pipe heat exchangers, and plate heat exchangers. Plate heat exchangers, as the name suggests, consist of several thin, usually rectangular metal plates pressed together in close proximity. The gaps between individual plates allow for two fluids to flow through on alternating sides of the plate and exchange heat, as illustrated in Figure 1.2 (Wang et al., 2007, p. 12). Loval mainly produces brazed plate heat exchangers, where the plates are brazed together using copper, in order to create a self-contained unit. These exchangers can handle higher pressures and temperatures compared to a gasket plate heat exchanger, where the plates are separated by a rubber gasket. They are however limited in size, usually shorter than one meter, due to brazing furnace constraints (Wang et al., 2007, pp. 17–18).

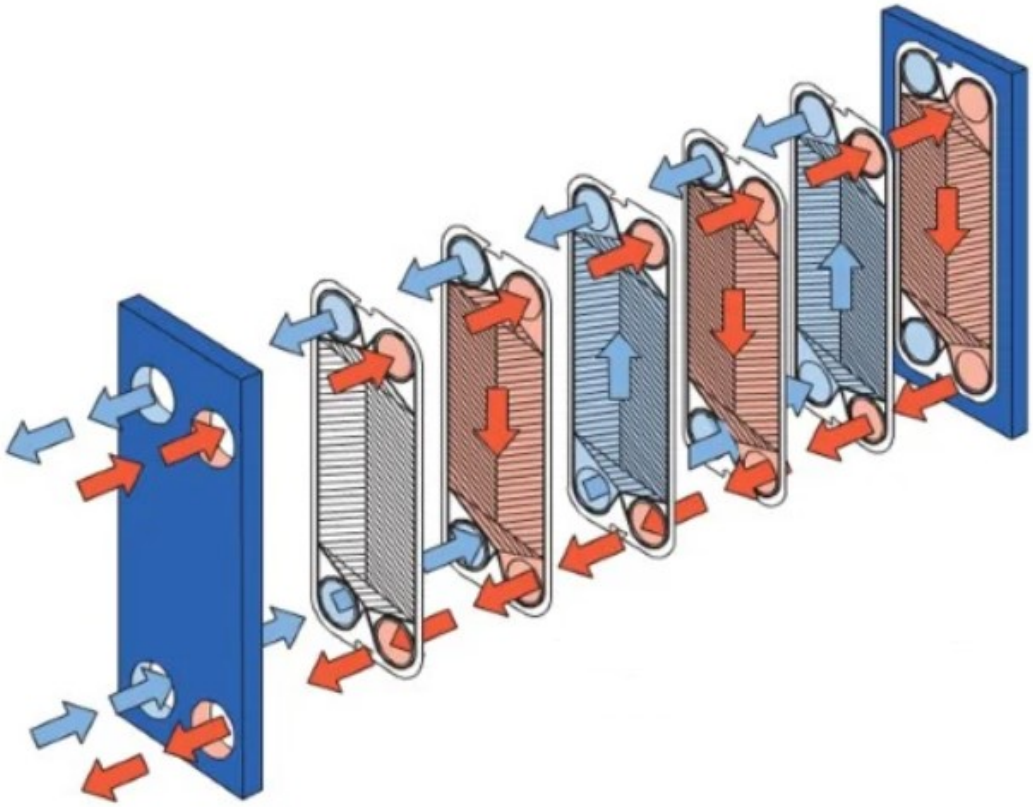

Figure 1.2. Flow principle of a gasket plate heat exchanger operating in a countercurrent configuration (Alfa-Laval, n.d.).

1.2 Calculation software

A significant portion of time is spent dimensioning and designing heat exchangers for customers. It is, therefore, in Loval's interest to develop a software tool that automates this process as much as possible. Given input values from the customer regarding the mass flows of the fluids and the inlet and outlet temperatures, this program ought to be able to calculate the necessary parameters to design a suitable heat exchanger.

A common type of heat exchanger sold at Loval is a brazed plate heat exchanger dimensioned for water-water use. Other fluids may include different oils and coolants. In order to be a useful application for Loval, this software must, at minimum, be able to take in data such as temperature and volume flow about two separate streams of water. Using predefined parameters from the most common heat exchangers at Loval, it should be able to calculate the inlet and outlet temperatures of the two streams, their respective volume

flows, the total heat flux, and the number of plates needed for a specific exchanger design, that is to say the total plate area. Once this basic framework has been built, additional features can be added, such as the ability to switch in different heat exchanger units with different design parameters, the ability to use different fluid combinations, such as water-oil or water-glycol, and the option to use different flow configurations.

If the previously mentioned features can be implemented, another thing to consider is the ability for users to add new heat exchanger designs and new fluids with different parameters. It is also of interest to develop a tool to produce printable reports containing central information regarding a calculation that can be used when producing a quotation for a customer. Once the back end of the software is functional, a graphical user interface will be designed in order to make the program more accessible. The possibility for a web-based user interface for potential customers will also be investigated.

1.3 Data collection

The output data from the calculation tool must be verifiable in order to be useful. Relatively simple equations exist in order to calculate the theoretical values for a heat exchanger with specified fluid flows and design parameters. One difficult aspect is estimating the internal fluid flow patterns, which are vital in order to calculate the overall heat transfer coefficient U. Small errors in the fluid flow characteristics can lead to large errors in the area estimate for the heat exchanger, especially in situations where the mean temperature differences between the hot and the cold flows are minute. Estimates with temperature differences of just a few degrees are typically more prone to errors.

Once a reasonable model has been built, a correction factor can be introduced in order to adjust the heat transfer area estimate. A set of experiments will be conducted on site at Loval in Loviisa where different heat exchanger designs will be tested with a variety of fluid flows in order to gather data about their performance. There are a number of different techniques used to fit a theoretical model to experimental data, one of them being the Wilson plot method (Fernández-Seara et al., 2007, p. 2745). The feasibility of utilizing the aforementioned method among others will be investigated.

The experimental setup illustrated in Figure 1.3 consist of two pumps feeding water from a hot buffer and a cold buffer tank into the heat exchanger one wishes to test.

The hot buffer tank is heated by an electric resistor, and the cold buffer tank is cooled through a separate loop. Pressure and temperature sensors on both sides of the heat exchanger allow for accurate readings, and flow sensors display the volumetric flow rate.

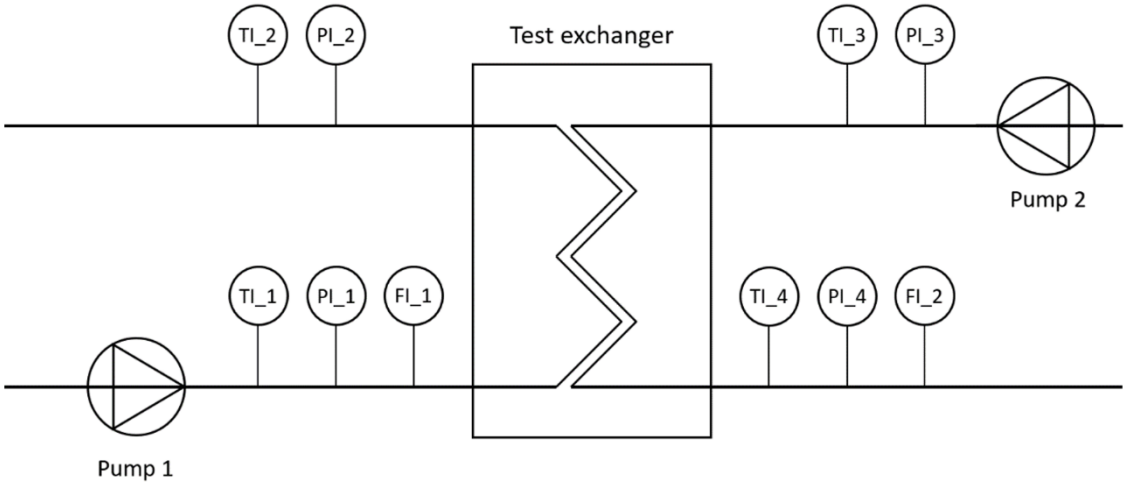

Figure 1.3. Experimental setup for testing heat exchangers.

2 Theory

As heat is transferred from one medium flow to another, the rate of heat flow $\dot{Q}$ is determined by the following energy balance:

$$\dot{Q} = \dot{m}\, c_p\, \Delta T \tag{1}$$

(Sekulić and Shah, 2003, p. 83)

Here $\dot{m}$ is the mass flow, c_p is the specific heat capacity, and ΔT is the temperature difference between the outgoing and ingoing stream. The values of either the hot or the cold side can be used, as the heat losses to the surrounding is miniscule for well-insulated units.

The total thermal energy passing through the surface wall between the two fluids, or the heat transfer rate, is determined by

$$\dot{Q} = U\, A\, \Delta T_m \tag{2}$$

(Sekulić and Shah, 2003, p. 83)

In this case U is the overall heat transfer coefficient, A is the heat transfer surface area, and ΔT_m is the logarithmic mean temperature difference. ΔT_m is a function of the inlet and outlet temperatures of both the hot and the cold streams, and is determined in the following way:

$$\Delta T_m = \frac{\Delta T_A - \Delta T_B}{ln\left(\frac{\Delta T_A}{\Delta T_B}\right)} \tag{3}$$

In this case ΔT_A and ΔT_B are the temperature differences at the ends of the exchanger, as seen in Figure 2.1.

When dimensioning a plate heat exchanger, the end goal is to solve for A in equation (2). Individual plates have a given area per plate, so once A is known, the total number of plates can be determined. This leaves U as the only parameter that must be determined before the problem can be solved. U is a function of the heat transfer characteristics of the two media with the plate, and the characteristics of the plate material in-between.

2.1 Flow configurations

Many plate heat exchangers can be run in either a co-current or a countercurrent configuration. Depending on the fluids in question, one mode may be preferable to the other, but for the most part a countercurrent configuration is used for reasons that will be discussed in coming chapters.

2.1.1 Co-current flow

In a co-current arrangement, the fluids enter and exit at the same ends and travel in the same direction through the heat exchanger as seen in Figure 2.1. This configuration has the lowest thermal efficiency of the mentioned configurations due to large deviations from the ideal constant temperature difference ΔT, and is incapable of heating the cold fluid above the outlet temperature of the hot fluid. The high temperature difference at the inlet also induces thermal stress across the exchanger wall, which might result in a reduced lifespan (Sekulić and Shah, 2003, pp. 58–59).

One possible advantage of a co-current configuration is that it results a more uniform temperature distribution across the heat exchanger when compared to other arrangements. When dealing with temperature sensitive materials, this aspect might be of importance when one considers extremely hot inlet flows in excess of about 1000 °C, as the combined temperature at the inlet will be lower when compared with a countercurrent arrangement (Sekulić and Shah, 2003, pp. 59–60).

2.1.2 Countercurrent flow

In a countercurrent arrangement, the fluids travel through the heat exchanger in opposite directions to one another as seen in Figure 2.1. This arrangement is the most efficient configuration due to a more uniform temperature difference, resulting in the highest transfer of thermal energy between the streams. Another benefit to the uniform temperature difference is the reduced thermal stress across the surface wall compared to other flow arrangements (Sekulić and Shah, 2003, p. 57).

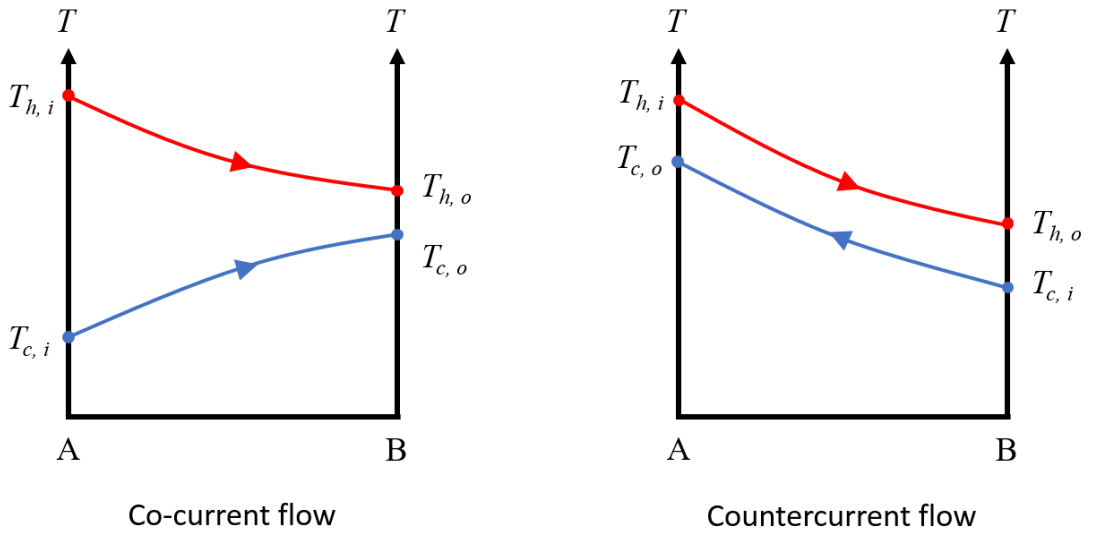

Figure 2.1. Temperature graph for co-current and countercurrent configurations

2.1.3 Cross flow

Heat exchangers can also be designed as cross flow exchangers. In this design, the hot and the cold side flow at a 90-degree angle to one another. Thermodynamically, this design is more efficient than a cocurrent configuration, but not quite as effective as a countercurrent design (Sekulić and Shah, 2003, p. 60).

Cross flow designs can usually be found in extended surface exchangers, or 2-phase heat exchangers, such as car radiators, where air flows perpendicular to the liquid coolant.

2.2 Exchanger parameters

In order to accurately calculate the Reynold number, Nusselt number, fluid velocity, and other variables, one needs to have detailed information regarding the properties and dimensions of the heat exchanger in question. The accuracy of these parameters is of paramount importance, as small deviations can lead to noticeable differences in flow and heat transfer characteristics, leading to unreliable outputs. The Reynold and Nusselt numbers are dimensionless numbers properly introduced in chapter 2.4. Figure 2.2 illustrates the most important dimensions of a chevron plate heat exchanger.

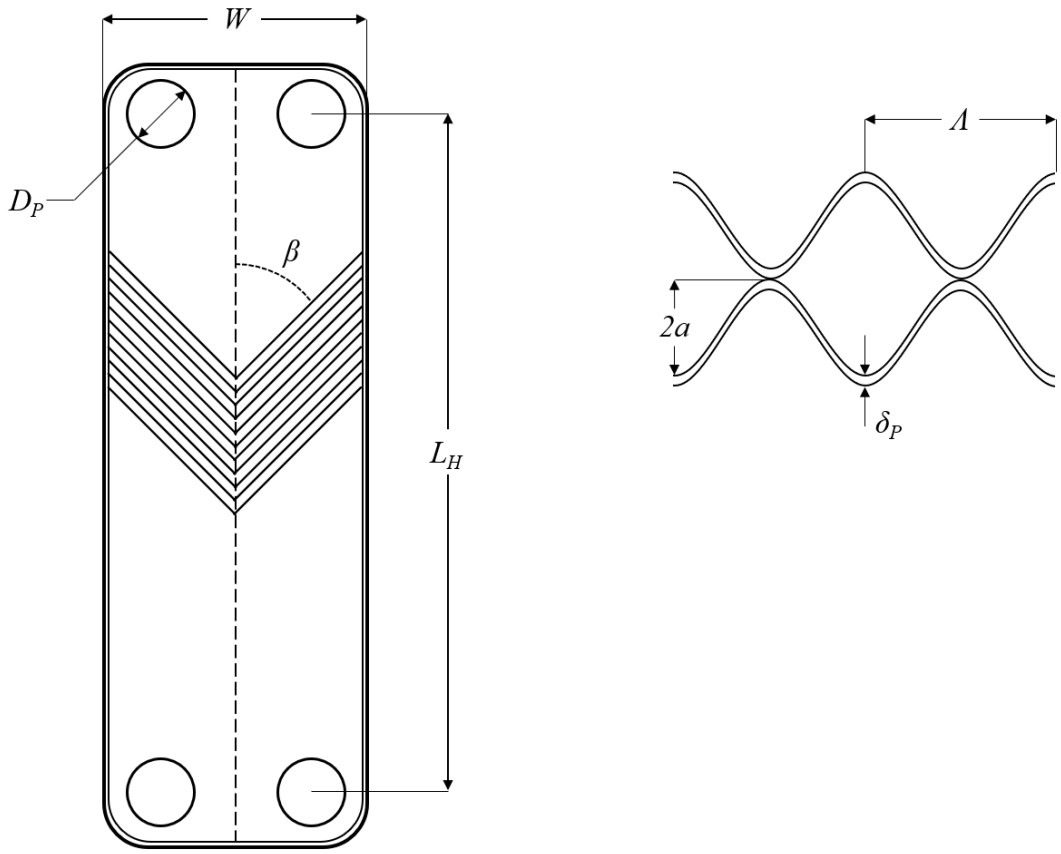

Figure 2.2. Chevron plate heat exchanger dimensions

2.2.1 Heat transfer area per plate

Most plates have complex engravings in order to manipulate flow patterns and increase the heat transfer area, and for this reason a more sophisticated way of estimating the transfer area is needed than just multiplying the plate width with the fluid flow distance. For the chevron pattern, one can estimate the ratio between the effective heat transfer area and an equivalent plain plate using the following equation:

$$\Phi \approx \frac{1}{6}\left(1+\sqrt{1+\left(\frac{2a\pi}{\Lambda}\right)^2}+4\sqrt{1+\frac{\left(\frac{2a\pi}{\Lambda}\right)^2}{2}}\right) \tag{4}$$

Thus, the effective heat transfer area can be estimated using the plate width, effective plate length and wave height (Martin, 1996, p. 302).

$$A = \Phi(WL_H + 2aL_H) \tag{5}$$

2.2.2 Hydraulic diameter

The hydraulic diameter D_H of the channels between two plates is an important parameter when estimating the overall heat transfer coefficient, and is defined according to

$$D_H = \frac{4A_c}{P_p} \tag{6}$$

where P_p is the wetter perimeter of the cross-sectional area A_c. D_H is easily determined in cases where the channel is cylindric or square, as A_c and P_p are well defined in those cases. When a chevron plate design is used, approximations have to be made. Using the previously defined surface correction factor, the hydraulic diameter can be determined.

$$D_H = \frac{4a}{\Phi} \tag{7}$$

(Sekulić and Shah, 2003, p. 597)

2.2.3 Additional parameters

In addition to the aforementioned parameters, an accurate list of other measurements that can only be found in detailed drawings are also needed in order to build a reliable model. The plate material determines the thermal conductivity, and is usually a stainless steel such as EN 1.4301 or EN 1.4404. Specifics about the chevron corrugation including the chevron angle β help determine the flow pattern, as does the size of the fittings.

2.3 Fluid parameters

The most common fluid used in heat exchangers is liquid water. Other fluids that Loval deals with are different hydraulic oils, antifreezes such as propylene glycol and ethanol, and steam in two-phase exchangers. The hydraulic oils that are of interest to Loval are primarily VG-32, VG-46, and VG-68. These fluids have some properties that can be copied from a datasheet at a given condition, but others vary drastically depending on the temperature and pressure. These variations can lead to vastly different outputs if neglected, so it is important to use values at the correct temperature and pressure.

2.3.1 Viscosity

The dynamic viscosity μ is important when dimensioning many different aspects of the heat exchanger, and for most fluids it varies with temperature. It is a measure of the internal resistance to deformation during flow, and it comes into play when calculation the Reynold number for example. Higher viscosities lead to less turbulent flows, meaning worse heat transfer. Depending on the context, viscosity can refer to dynamic viscosity μ, or kinematic viscosity v. Care should be taken not to mix up these two separate measurements. The dynamic viscosity can be calculated by multiplying the kinematic viscosity with the density.

The following equation can be used for determining the dynamic viscosity of liquid water as a function of temperature.

$$\mu(T) = 2.414 \cdot 10^{-5} Pas \cdot 10^{\left(\frac{247.8K}{T-140K}\right)} \tag{8}$$

Here T is the temperature in Kelvin. When estimating the mean dynamic viscosity for a fluid in a heat exchanger, one cannot use the viscosity at the mean temperature, as μ usually does not vary linearly with respect to temperature. Instead, a more accurate value for water can be obtained by integrating equation (8) and setting the limits as the inlet and outlet temperature, and dividing the result by the temperature difference. The dynamic viscosity for water varies between 0.00175 Pa·s and 0.000279 Pa·s at T = 0° C and T = 100° C.

Figure 2.3 illustrates how the viscosity of different hydraulic oils vary with respect to temperature. Separate equations describing the relationship can be constructing by curve fitting a polynomial function to individual datapoints for each fluid in Figure 2.3. Compared to water, the viscosity of hydraulic oils vary even more drastically with temperature, and can almost change by almost two orders of magnitude between T = 0° C and T = 100° C (Shell-Oil-Company, 2010).

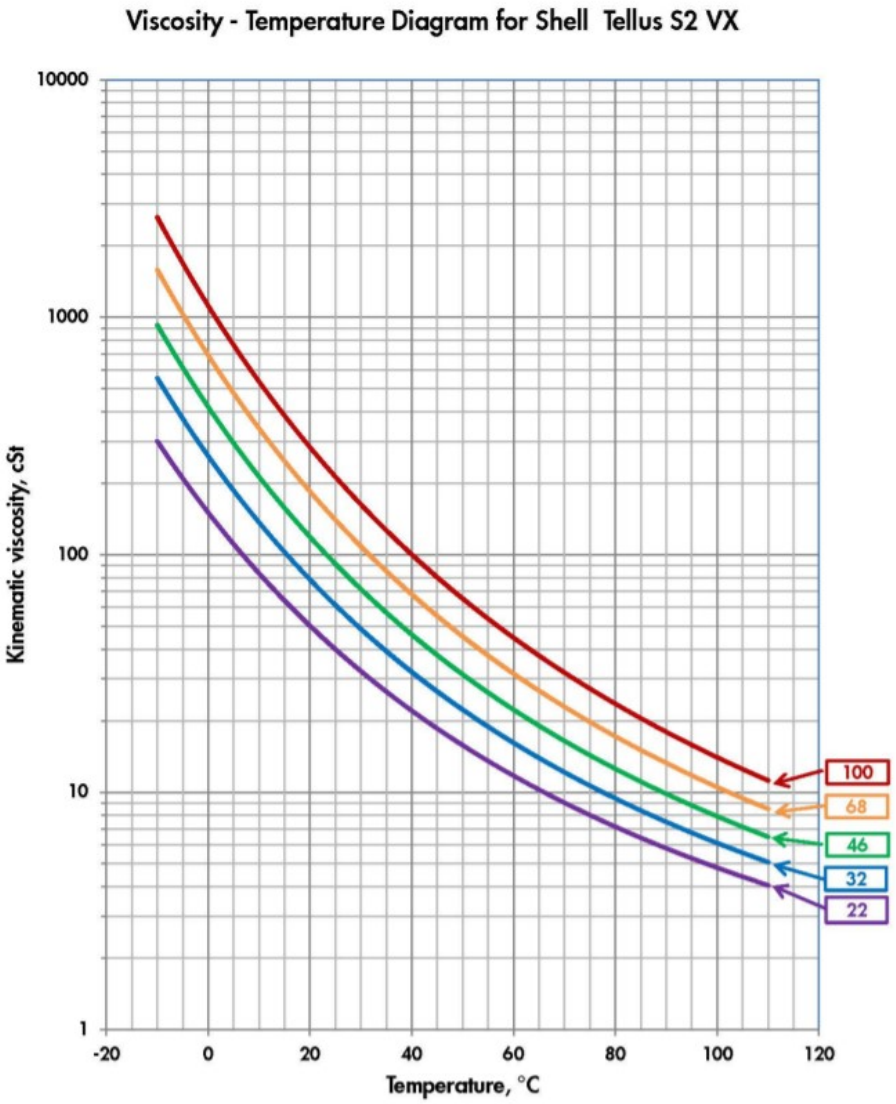

Figure 2.3. Kinematic viscosity of different hydraulic oils (Shell-Oil-Company, 2010). The colored lines represent the hydraulic oils VG-22, VG-32, VG-46, VG-68, and VG-100.

2.3.2 Thermal conductivity

Another property that varies with temperature is the thermal conductivity k. For liquid water, Kays et al. provide the following estimate.

$$k(T) = -8.354 \cdot 10^{-6}T^2 + 6.53 \cdot 10^{-3}T - 0.5981 \quad (9)$$

(Kays et al., 2005)

Here T is the temperature in Kelvin. Between T = 0° C and T = 100° C, the conductivity varies from 0.563 W/mK to 0.675 W/mK. This difference can be significant enough to cause noticeable variations in the overall heat transfer coefficient U if omitted.

2.3.3 Density

Density is also dependent on the fluid temperature, although it does not vary as drastically as thermal conductivity or especially viscosity for most liquids. Using tabulated values for the density of water at different temperatures (United-States-Geological-Survey, n.d.), the following polynomial function was constructed using regression analysis.

$$\rho(T) = 1.031 \cdot 10^{-12}T^5 - 3.4942 \times 10^{-10}T^4 + 5{,}708 \cdot 10^{-8}T^3 - 7{,}950 \cdot 10^{-6}T^2 + 5{,}837 \cdot 10^{-5}T + 0.9999 \quad (10)$$

Here T is the temperature is Celsius.

2.3.4 Heat capacity

Temperature has a minimal effect on the heat capacity for most fluids in the relevant temperature ranges. c_p varies from 4.17 kJ/kgK to 4.21 kJ/kgK for liquid water. This small change of less than 1% can be neglected when performing calculations.

2.4 Overall heat transfer coefficient

The overall heat transfer coefficient in a heat exchanger is dependent upon the characteristics of the plate material, the convective heat transfer coefficient of both the cold and the warm fluid, and any fouling between the plate and the fluids. This coefficient is defined accordingly:

$$U = \left(\frac{1}{\alpha_h} + \frac{\delta_P}{k_P} + \frac{1}{\alpha_c} + R_{f,h} + R_{f,c}\right)^{-1} \quad (11)$$

(Wang et al., 2007, p. 56)

Here α_h and α_c are the convective heat transfer coefficients for the hot and cold fluids, δ_P is the thickness of the plate, k_P is the thermal conductivity of the plate, and $R_{f,h}$ as well as $R_{f,c}$ are the fouling resistances on both sides of the plate. Unless otherwise specified, these

fouling resistances are assumed to be zero. Both δ_P and k_P are usually well defined, so only the fluids convective heat transfer coefficients needs to be determined.

By utilizing the definition of the Nusselt number, α can be described in the following way:

$$\alpha_i = \frac{k_i \mathrm{Nu}}{D_H} \tag{12}$$

Here k_i is the thermal conductivity of the flowing fluid in question. Nu can be difficult to determine due to the complex geometries present inside a chevron plate heat exchanger. A commonly used estimate today is an updated version of an estimate obtained by Martin (1996) specifically for chevron plate heat exchangers in 1996.

$$\mathrm{Nu} = 0.205 \mathrm{Pr}^{\frac{1}{3}} \left(\frac{\mu_m}{\mu_w}\right)^{\frac{1}{6}} \left(f \mathrm{Re}^2 sin(2\beta)\right)^{0.374} \tag{13}$$

(Sekulić and Shah, 2003, p. 515)

Here Pr is the Prandtl number, Re is the Reynold number, β is the chevron corrugation angle, and f is the Fanning friction factor. The friction factor also comes into play when determining the pressure drops inside the heat exchanger. μ_m and μ_w denote the fluids dynamic viscosity at the medium's temperature and at the wall temperature, respectively. Other more recent estimates for the Nusselt number are presented in chapter 2.5.

Pr is wholly dependent on the fluid itself and is easily determined. It is defined as the ratio between the momentum diffusivity and the thermal diffusivity.

$$\mathrm{Pr} = \frac{c_p \mu}{k} \tag{14}$$

In order to get accurate estimates for U in different fluid configurations, one must consider how the viscosity and thermal conductivity of the fluids vary at different temperatures. The Prandtl number can be anywhere from 1.5 to 12 for liquid water at atmospheric pressure.

Re describes the flow patterns for a fluid in different geometries and at different velocities, and is dependent on both the pipe characteristics and fluid parameters, as well as the tube cross-sectional average velocity u.

$$\mathrm{Re} = \frac{\rho u D_H}{\mu} \tag{15}$$

At low Re values internal viscous forces dominate, resulting in laminar flow, while at high Re values inertial forces dominate, leading to turbulent flow. Turbulent flow is often intentionally introduced with the help of irregularities on the surface of the heat transfer plate, as this improves the thermal efficiency of the heat exchanger. This also results in larger pressure drops inside the exchanger, but this tradeoff is usually worthwhile depending on the intended application.

2.5 Nusselt number

No common estimation for the Nusselt number for plate heat exchangers exists in the available literature (Zahid, 2003, p. 8). Instead, a commonly used method to estimate the heat transfer is to utilize the Wilson plot technique (Opatřil et al., 2016, p. 369) (Asif et al., 2017, p. 208). Here, experimentally obtained data are used to estimate parameter values for the following generalized version of the Sieder-Tate correlation (Sieder and Tate, 1936, pp. 1429–1435):

$$\mathrm{Nu} = C\mathrm{Re}^m\mathrm{Pr}^n\left(\frac{\mu}{\mu_w}\right)^{0.14} \tag{16}$$

Here *C*, *m*, and *n* are the parameters in question. This method is, however, limited by the experimental data available, and the predicted solution tends to show large discrepancies if applied to a plate with slightly different parameters (Dović et al., 2009, p. 4553). The Wilson plot technique is properly introduced in chapter 2.8.

In an effort to develop a more theoretical solution, Dović et al. (2009) attempted to model the fluid characteristics inside an individual cell, as depicted in Figure 2.4. By considering both the longitudinal and furrow components of the flow for different plate geometries, they arrived at the following Nusselt number estimate for an individual sine duct:

$$Nu_{sine} = C_1(C + Re_{sine}B)^{0.375}{Re_{sine}}^{0.375}Pr^{\frac{1}{3}}\left(\frac{\mu}{\mu_w}\right)^{0.14} \tag{17}$$

(Dović et al., 2009, p. 4559)

Here C_1, C, and B are parameters dependent on the chevron wave height $2a$, and the chevron wavelength Λ. These parameters can be determined by calculating

$$\begin{cases} f_{fully}Re_{sine} = 2.6624\left(\frac{2a}{\Lambda}\right)^4 - 10.586\left(\frac{2a}{\Lambda}\right)^3 + 11.252\left(\frac{2a}{\Lambda}\right)^2 - 1.0103\left(\frac{2a}{\Lambda}\right) + 9.6 \\ K_e(\infty) = -5.888\left(\frac{2a}{\Lambda}\right)^4 + 9.4613\left(\frac{2a}{\Lambda}\right)^3 - 4.248\left(\frac{2a}{\Lambda}\right)^2 - 0.1333\left(\frac{2a}{\Lambda}\right) + 2.648 \\ K_d(\infty) = -1.7237\left(\frac{2a}{\Lambda}\right)^4 + 2.7669\left(\frac{2a}{\Lambda}\right)^3 - 1.2651\left(\frac{2a}{\Lambda}\right)^2 - 0.0097\left(\frac{2a}{\Lambda}\right) + 1.512 \end{cases} \quad (18)$$

and

$$\begin{cases} K(\infty) = 2[K_e(\infty) - K_d(\infty)] \\ d_{h,sine} = \Lambda\left(0.1429\left(\frac{2a}{\Lambda}\right)^3 + 0.6235\left(\frac{2a}{\Lambda}\right)^2 + 1.0871\left(\frac{2a}{\Lambda}\right) - 0.0014\right) \end{cases} \quad (19)$$

as well as

$$\begin{cases} L_{cell} = \dfrac{\Lambda}{\sin(2\beta)} & when\ \beta \leq 60° \\ L_{cell} = \dfrac{\Lambda}{\sin(\beta)} & when\ \beta > 60° \end{cases} \quad (20)$$

(Dović et al., 2009, p. 4557)

From here on the parameters C_1, C, and B can be determined by utilizing equations (18) through (20).

$$\begin{cases} C_1 = 0.25804\left(\dfrac{d_{h,sine}}{L_{cell}}\right)^{0.375} \\ C = f_{fully}\mathrm{Re}_{sine} \\ B = \dfrac{K(\infty)d_{h,sine}}{4L_{cell}} \end{cases} \quad (21)$$

(Dović et al., 2009, p. 4559)

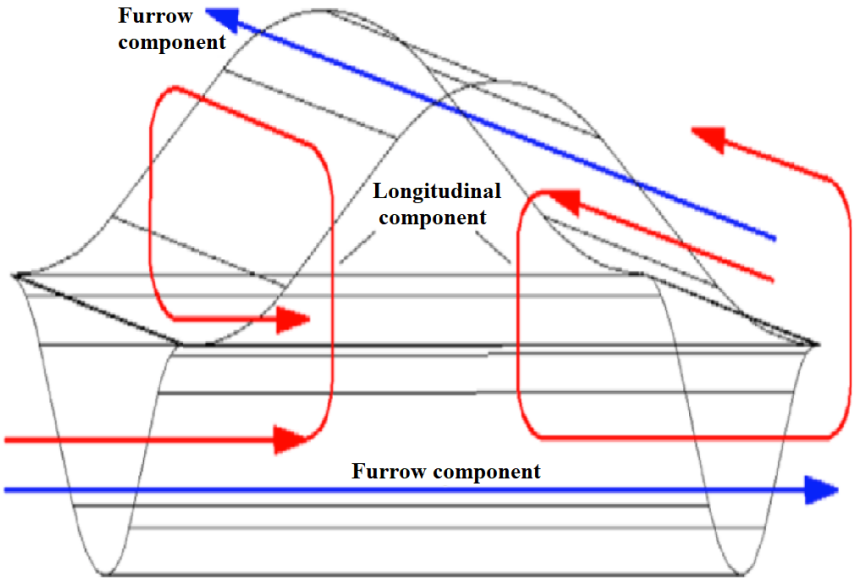

Figure 2.4. Fluid component flows through an individual cell in a chevron plate heat exchanger (Dović et al., 2009, p. 4555).

The Reynold number in an individual sine duct is calculated in the usual manner, except in this case D_H is replaced by $d_{h,\,sine}$, and the velocity through the sine duct is determined as follows:

$$u_{sine} = \frac{\dot{m}}{\rho W 2a\, cos(\beta)\, n_c} \tag{22}$$

Here $\dot{m}$ is the total fluid mass flow, ρ is the density, W is the plate width, and n_c is the number of channels. A Reynold number ratio for the entire heat exchanger is defined as a ratio between the tube cross-sectional average velocity and the hydraulic diameter for a single sine section, and the tube cross-sectional average velocity and the hydraulic diameter for the whole unit.

$$\frac{\mathrm{Re}_{sine}}{\mathrm{Re}} = \frac{u_{sine} d_{h,sine}}{u D_H} = \frac{d_{h,sine}}{D_H\, cos\, \beta} \tag{23}$$

The Nusselt number for an individual sine section can then be calculated, and the Nusselt number for the entire heat exchanger can be determined in a similar manner as the Reynold number.

$$\frac{\mathrm{Nu}}{\mathrm{Nu}_{sine}} = \frac{D_H}{d_{h,sine}} \tag{24}$$

(Dović et al., 2009, p. 4558)

Dović et al. note that this analytical solution shows relatively large deviations from experimentally determined Fanning friction factor values ± (10-50) %, and that this is mainly due to the lack of an empirical correction factor. Such a correction factor can be difficult to obtain as the experimental data available typically contain large discrepancies (Dović et al., 2009, p. 4562).

2.6 Friction factor

The Fanning friction factor *f* is defined as the ratio between the shear stress and the kinetic energy density of the fluid flow, and can be interpreted as the resistance to flow caused by the fluid moving through a channel. It is defined as

$$f = \frac{\tau}{\rho \frac{u^2}{2}} \tag{25}$$

where τ is the shear stress. It is highly dependent on the specific geometry through which the fluid flows, and it is also dependent on the flow characteristics of the fluid itself. Another coefficient for the friction is the Darcy friction factor f_D that is defined accordingly.

$$f_D = 4f \tag{26}$$

One must take care not to confuse these two factors, as both are commonly used in the literature.

A number of different estimations for the friction factor in chevron plate heat exchangers have been suggested over the years. These estimations can vary from one another by over one order of magnitude, as seen in Figure 2.5, showcasing that a commonly agreed upon and consistent method to predict the internal friction factor does not exist. This is in part due to highly inconsistent databases, where experimentally measured friction factors can vary up to five-fold at similar Reynolds values (Zhu and Haglind, 2020, p. 2).

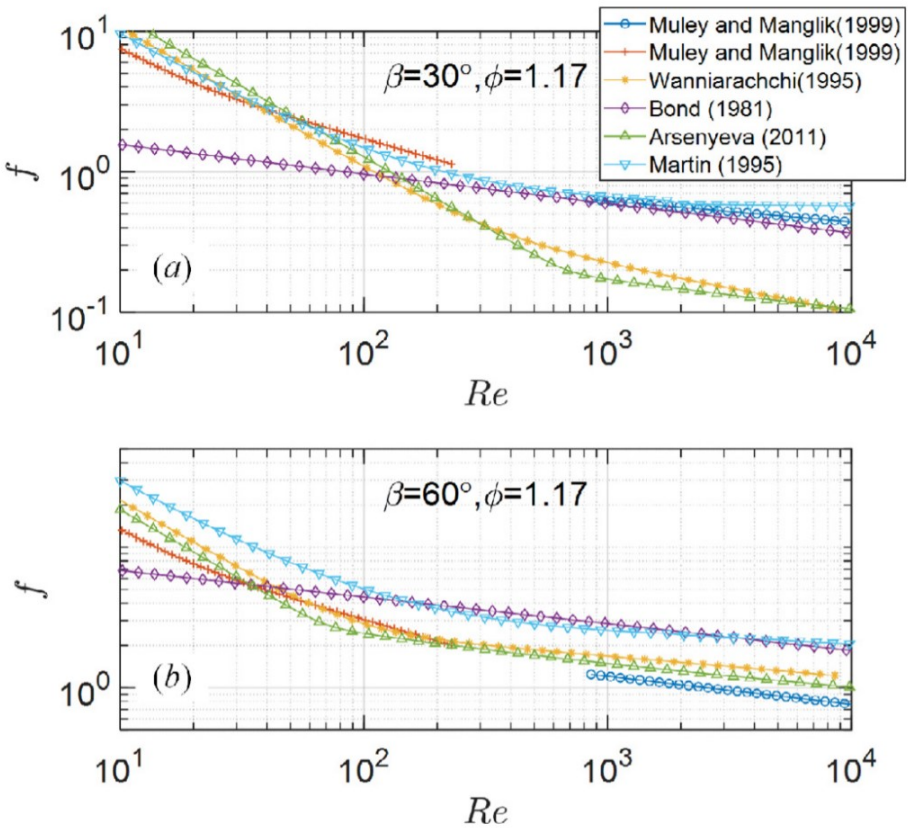

Figure 2.5. Prevalent assessments for f_D in plate heat exchangers (Zhu and Haglind, 2020, p. 3).

A commonly used estimate for the friction factor is the following one developed by Martin in 1996:

$$\frac{1}{\sqrt{f}} = \frac{\cos(\beta)}{\left(0.045tan(\beta) + 0.09sin(\beta) + \frac{f_0}{\cos(\beta)}\right)^{0.5}} + \frac{1-\cos(\beta)}{\sqrt{3.8f_1}} \tag{27}$$

Here f_0 and f_1 are additional parameters which are dependent on Re in the following way:

$$f_0 = \begin{cases} \frac{16}{\mathrm{Re}} & for\ Re < 2000 \\ (1.56ln(Re) - 3)^{-2} & for\ Re \geq 2000 \end{cases} \tag{28}$$

$$f_1 = \begin{cases} \frac{149.25}{Re} + 0.9625 & for\ Re < 2000 \\ \frac{9.75}{\mathrm{Re}^{0.289}} & for\ Re \geq 2000 \end{cases} \tag{29}$$

(Martin, 1996, pp. 301–310)

Martin states that this friction factor is valid for chevron angles between 0 and 80°, and the predicted Darcy friction factor for β = 60° and β = 30° is shown in Figure 2.5 under the legend "Martin (1995)".

Thanks to rapid advancements in computer technology, computational fluid dynamics has now become an invaluable tool when modeling and predicting fluid flows. Using the Large Eddy Simulation, Zhu and Haglind simulated fully developed flows in the channels of cross-corrugated chevron plates for 18°< β <72° (Zhu and Haglind, 2020, p. 1). Using the Colebrook equation that is used to plot the turbulent section in the Moody diagram, Zhu and Haglind modified it by assuming that the chevron angle can be modeled as a kind of surface roughness. They obtained the following estimate for f_D by curve fitting data from their CFD simulations:

$$\frac{1}{\sqrt{f_D}} = -2.0log_{10}\left(1.48\,sin(\beta)^{4.85}\,cos(\beta)^{0.45} + \frac{60\,sin\,2\beta^3\,cos\,\beta^5 + 16}{\mathrm{Re}\sqrt{f_D}}\right) \quad (30)$$

(Zhu and Haglind, 2020, p. 6)

The theoretical model of an individual chevron cell developed by Dović et al. also predicts a value for the friction factor across the whole channel. The friction factor inside an individual cell can be determined with the Reynold number for a single sine section, and the parameters *B* and *C* accordingly.

$$f_{sine} = \frac{C}{\mathrm{Re}_{sine}} + B \quad (31)$$

The overall Fanning friction factor is then estimated as a fraction between the individual cell and the whole channel:

$$\begin{cases} f = \dfrac{D_H f_{sine}}{d_{h,sine} 2cos^3(\beta)} & when\ \beta \leq 60° \\ f = \dfrac{D_H f_{sine}}{d_{h,sine} cos^2(\beta)} & when\ \beta > 60° \end{cases} \quad (32)$$

(Dović et al., 2009, p. 4558)

A comparison between the friction factor estimates from Martin, Dović et al., and Zhu & Haglind, with β = 60° and $2a/\Lambda$ = 0.304 is illustrated in Figure 2.6, and β = 70° in Figure 2.7. It can be noted that estimates from these formulas vary widely from one to

another at both small and large Reynold numbers. Zhu and Haglind's model was developed mainly in order to predict the friction factor in developed turbulent flows, but it still works surprisingly well in laminar regimes, and can be used there as well (Zhu and Haglind, 2020, p. 9). Experimental data are needed to validate the accuracy of these models in order to determine which one ought to be used in the calculation tool.

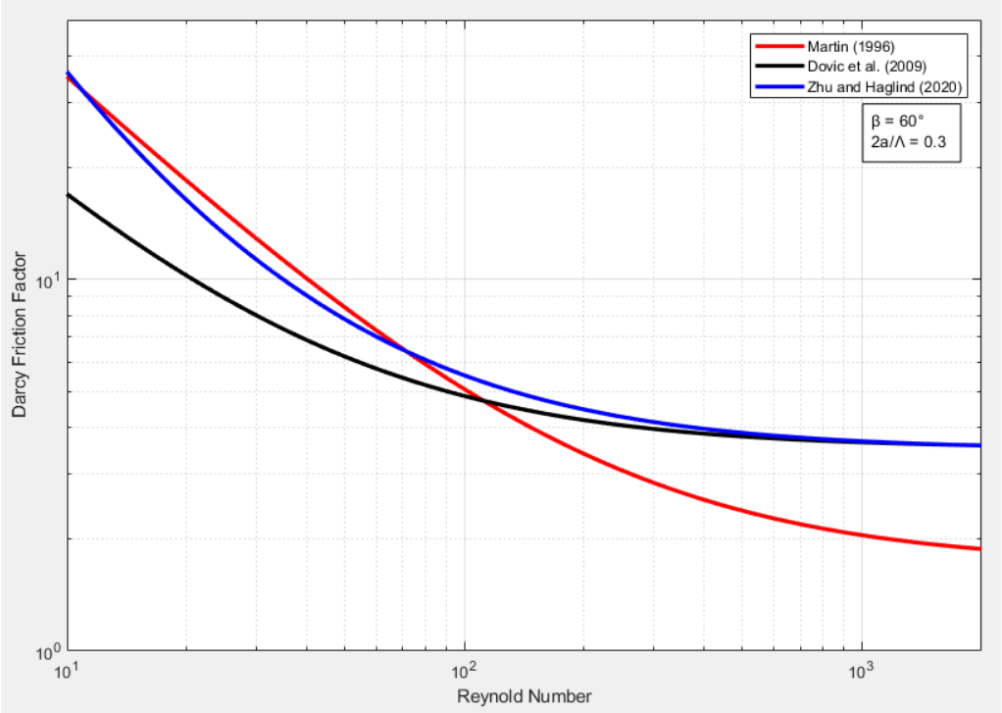

Figure 2.6. Darcy friction factor estimates for equation (26), (29) and (31) at $\beta = 60°$ and $2a/\Lambda = 0.304$.

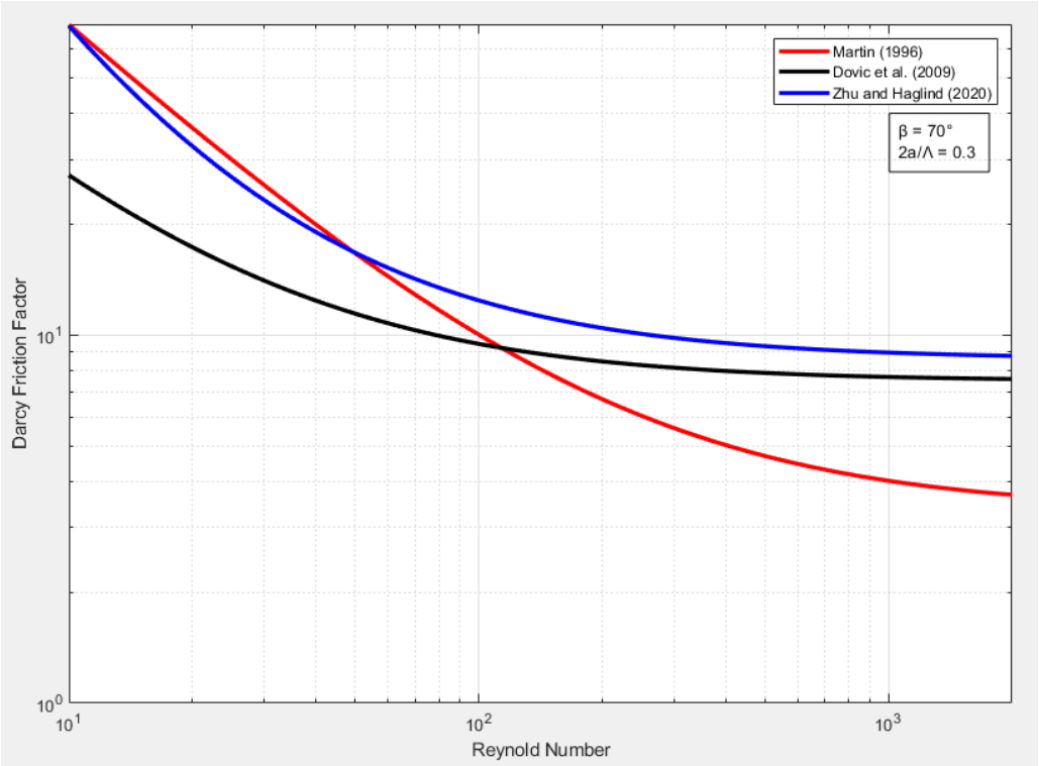

Figure 2.7. Darcy friction factor estimates for equation (26), (29) and (31) β = 70° and $2a/\Lambda$ = 0.304.

2.7 Pressure drop

When a fluid travels through a heat exchanger, it will inevitably result in a pressure drop between the inlet and outlet. This is important to consider, because the power needed to pump the fluid through the heat exchanger is proportional to the pressure drop over the system, and is given by

$$P = \frac{\dot{V}\Delta p}{\eta_p} \tag{33}$$

where $\dot{V}$ is the fluid volume flow and η_p is the pump or fan efficiency. This equation is valid for non-compressible fluids.

In a plate heat exchanger, the main sources of pressure drop manifest from the inlet and outlet ports, and from the core. The latter source of pressure drop is usually the largest, as a complex plate geometry is necessary to facilitate optimal heat transfer,

resulting in significant friction. The pressure drop from the inlet and outlet ports can be minimized by designing appropriately sized ports.

A small pressure change occurs as a result of the fluid density changing as the temperature rises or falls as it travels through the heat exchanger. Finally, there is also a pressure change if the fluid elevation changes due to the orientation of the heat exchanger. Adding up all these terms, the resulting equation is the following.

$$\Delta p = \frac{1.5{G_p}^2}{2\rho_i} + \frac{2fL_H G^2}{D_H \rho_m} + \left(\frac{1}{\rho_o} - \frac{1}{\rho_i}\right) G^2 \pm \rho_m g L_H \tag{34}$$

(Sekulić and Shah, 2003, p. 397)

Here ρ_i, ρ_o, *and* ρ_m stand for inlet, outlet and mean density, D_H is the hydraulic diameter, L_H is the vertical distance between the inlet and outlet port, and g is the gravitational constant. G_p and G are the fluid mass velocities through the port and through the core, and are calculated as follows:

$$G_p = \frac{\dot{m}}{\left(\frac{\pi}{4}\right){D_p}^2} \tag{35}$$

$$G = \frac{\dot{m}}{A_c n_c} \tag{36}$$

Here D_p is the port diameter, n_p is the number of channels, and A_c is the cross-sectional area in one channel.

When dealing with liquid flows, the pressure change resulting from density changes can be omitted. The pressure drops from elevation changes is usually accounted for elsewhere when designing the pipe systems, and should be mentioned separately. Pressure drops from the ports should ideally be kept under 10% of the total pressure drop, but it is not uncommon for it to exceed 20% (Sekulić and Shah, 2003, p. 397).

2.8 Wilson plot method

The methods for determining the Nusselt number and friction factor discussed in chapters 2.5 and 2.6 are only a few of the available estimates. In a literature survey, Zahid compiled a list of 28 different papers, all suggesting different values for the parameters C, m, and n for the generalized Sieder-Tate correlation (Sieder and Tate, 1936, pp. 1429–1435) (37), and all subject to different constrains for the Reynold number, Prandtl number, and chevron angle (Zahid, 2003, pp. 9–12).

$$\mathrm{Nu} = C\mathrm{Re}^{m}\mathrm{Pr}^{n}\left(\frac{\mu}{\mu_w}\right)^{0.14} \tag{37}$$

In order to build a tool capable of producing reliable outputs, it might best to construct separate Nusselt estimates for each heat exchanger model, instead of relying on one specific function like Martin's Nu estimate. These separate estimates can be constructed using the Wilson plot method.

2.8.1 Original Wilson plot method

The heat transfer in an exchanger can be described with the overall thermal resistance R_{ov}, instead of the overall heat transfer coefficient U.

$$\dot{Q} = \frac{\Delta T_m}{R_{ov}} \tag{38}$$

Here R_{ov} consists of the thermal resistance for both fluids, the thermal resistance for the plate, and the thermal resistance for the fouling on both sides of the plate.

$$R_{ov} = R_h + R_{f,h} + R_w + R_{f,c} + R_c \tag{39}$$

By conducting experiments where the flow characteristics of only one fluid is altered, say the cold side, the rest of the thermal resistance factors ought to remain unchanged, which means they can be described by a constant.

$$C_1 = R_h + R_{f,h} + R_w + R_{f,c} \tag{40}$$

If one neglects the variations in fluid properties due to changes in the temperatures, then the changes in the Nusselt number will be proportional to Re^m, and the thermal resistance of the fluid will be proportional to $1/ Re^m$.

$$R_c = C_2 \frac{1}{\mathrm{Re}^m} \tag{41}$$

By adding the constant thermal resistances C_1 and the resistance of the cold side R_c, the following equation for R_{ov} is obtained, which is just the equation for a straight line.

$$R_{ov} = C_1 + C_2 \frac{1}{\mathrm{Re}^m} \tag{42}$$

The results of the experiments can now be plotted on a graph with R_{ov} on the y-axis and $1/Re^m$ on the x-axis if a value for m is assumed. A linear function can then be fitted to the plotted data with a simple linear regression, and the values for C_1 and C_2 can be determined, as illustrated in Figure 2.8. Afterwards the values for the conductive heat transfer coefficients α_c and α_h as well as the constant C can be calculated in the following way.

$$\alpha_h = \frac{1}{\left(C_1 - A\left(R_{f,h} + R_w + R_{f,c}\right)\right)} \tag{43}$$

$$\alpha_c = \frac{\mathrm{Re}^m}{C_2 A} \tag{44}$$

$$C = \frac{1}{C_2 \left(\frac{k_c}{D_H}\right) \mathrm{Pr}^{0.4} A} \tag{45}$$

Here k_c is the thermal conductivity of the cold fluid.

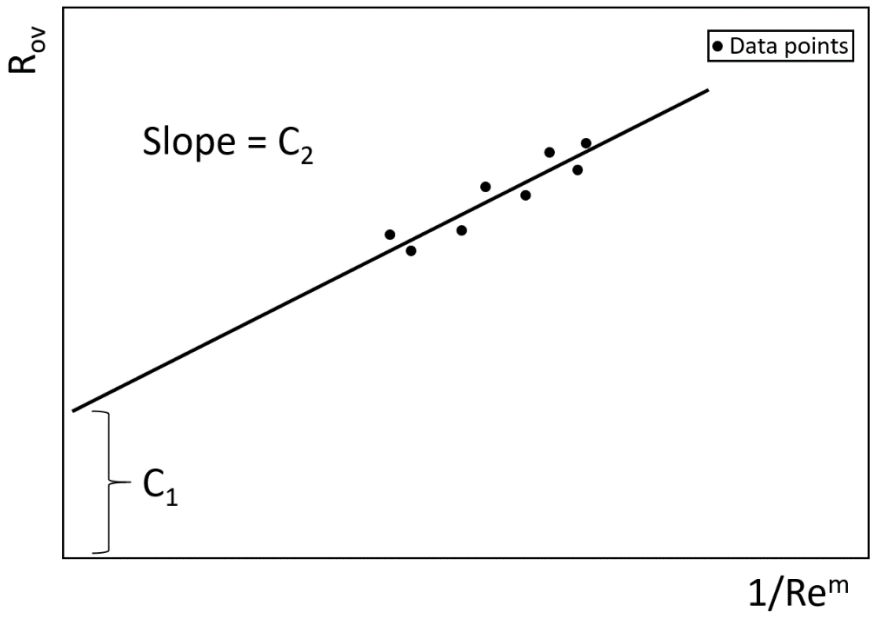

Figure 2.8. Plot of R_{ov} vs. $1/Re^m$.

2.8.2 Modified Wilson plot method

The value for the Reynold exponent *m* can also be determined by applying logarithms to both sides of equation (42).

$$ln\left(\frac{1}{R_{ov}-C_1}\right) = ln\left(\frac{1}{C_2}\right) + mln(\mathrm{Re}) \tag{46}$$

This equation also takes the form of a straight line, with *m* describing the slope. By plotting $ln[1/(R_{ov}- C_1)]$ as a function of $ln(\mathrm{Re})$ and using linear regression, a value for *m* can be obtained, as show in Figure 2.9. If this value is not equal to the initial assumption, then a new value for *m* is assumed, and the whole process is repeated (Fernández-Seara, Uhía and Sieres, 2007, pp. 123–135).

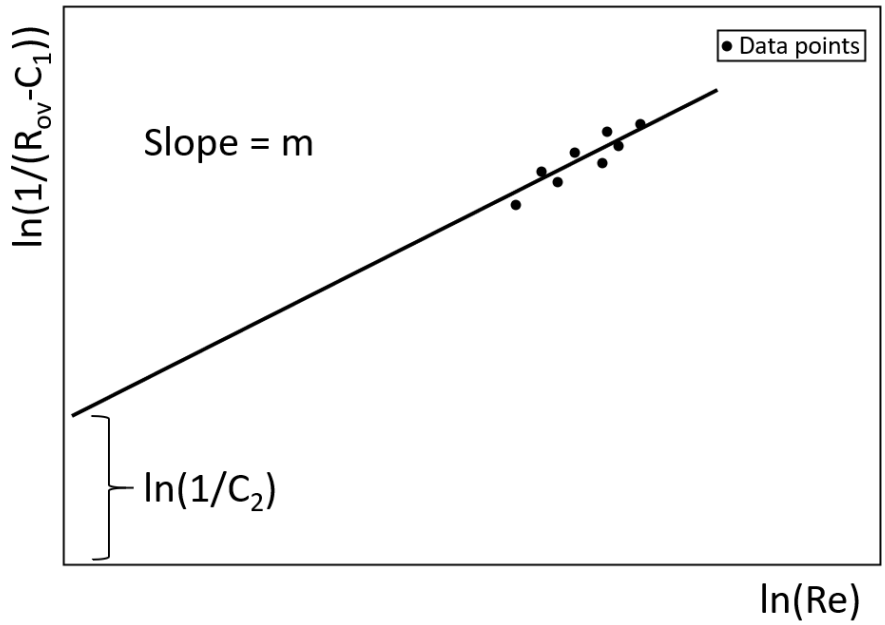

Figure 2.9. Plot of $\ln(1/(R_{ov} - C_1))$ vs. ln(Re).

2.8.3 Constraints

When conduction experiments and changing the flow rate in the cold stream, it is assumed that the Prandtl number for the cold stream, and the heat transfer coefficient for the hot stream stay constant. This is not obvious from the outset, because when the fluid flow rate increases, the outgoing temperature of the stream will be affected. This affects the dynamic viscosity of the fluid as well as the thermal conductivity, and thus the Prandtl number. The wall temperature will also change as a result, and this will induce a change in the heat transfer coefficient of the hot stream (Fernández-Seara et al., 2007, p. 2750). As a result, the observed change in the overall heat transfer coefficient will not purely be due to a change in the Reynold number for the cold stream.

The accuracy of the temperature and volume flow measurements also add significant constraints. Wójs and Tietze simulated interference in the temperature measurements used to calculate the heat transfer parameters and found that a mean-square deviation of just 0.1 K could lead to a ~ 20% error in the estimated heat transfer coefficient. In cases where the mean-square deviation is 1 K, the discrepancy between the real and the predicted results exceed 50%, and the method becomes practically unusable (Wójs and Tietze, 1997, pp. 244–245).

Rose lists several other constraints in his article, noting that the range of the gathered data determines what range the calculated parameters are valid in. There is also the risk of producing erroneous results if one attempts to determine too many parameters, especially if the accuracy and the number of datapoints do not justify this (Rose, 2004, p. 80).

3 Data collection

3.1 Experimental apparatus

3.1.1 Heat exchanger models

Experimental tests will be performed with three different heat exchanger models. These models are HP-33, HP-64, and HP-52B. The dimensions of these models are presented in Figure 3.1. 10-plate, 30-plate, and 60-plate versions of these models are included in the experiments, resulting in a total of nine different heat exchangers.

Dimensions (mm)	HP-52B	HP-64	HP-33
A	529	529	330
B	113	124	113
C	476	477	277
D	60	73	60
E	n*1,92+14	n*2,4+8	n*1,92+14

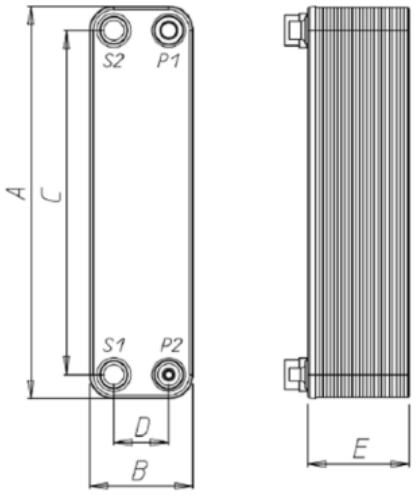

Figure 3.1. Dimensions of the three heat exchangers included in the tests (Loval Oy). Here *n* is the number of plates.

3.1.2 Test setups

Two different test setups will be used, one for heat transfer measurements, and one for pressure drop measurements. Figure 3.2 contains two images of the setup used for heat transfer measurements. The image on the left depicts the setup itself, where the two rightmost hoses are the inlet and outlet for the hot side, and the two hoses in the middle are the inlet and outlet for the cold side. The image on the right is taken during an experimental run with a 10-plate version of the HP-52B heat exchanger.

Figure 3.2. Setup used for heat transfer experiments.

In practice, water for the cold side is taken from a hand wash sink in order to quickly be able to make small adjustments to the inlet temperature, as the temperature controls in the actual setup are rather slow. The ability to measure the volume flow of the cold side is lost using this method, but it can be recalculated as all four inlet and outlet temperatures are measured alongside the hot sides volume flow. A Pico USB TC-08 is used to measure and log the temperatures on a computer during experiments.

An older setup is used for the pressure drop experiments as it has a more accurate pressure sensor. Figure 3.3 contains two images of this setup, one taken during an active run with a 60-plate version of the HP-52B heat exchanger. The experiments are set to run for a couple of minutes to ensure that an equilibrium has been reached before the measurements are taken and logged on a desktop computer.

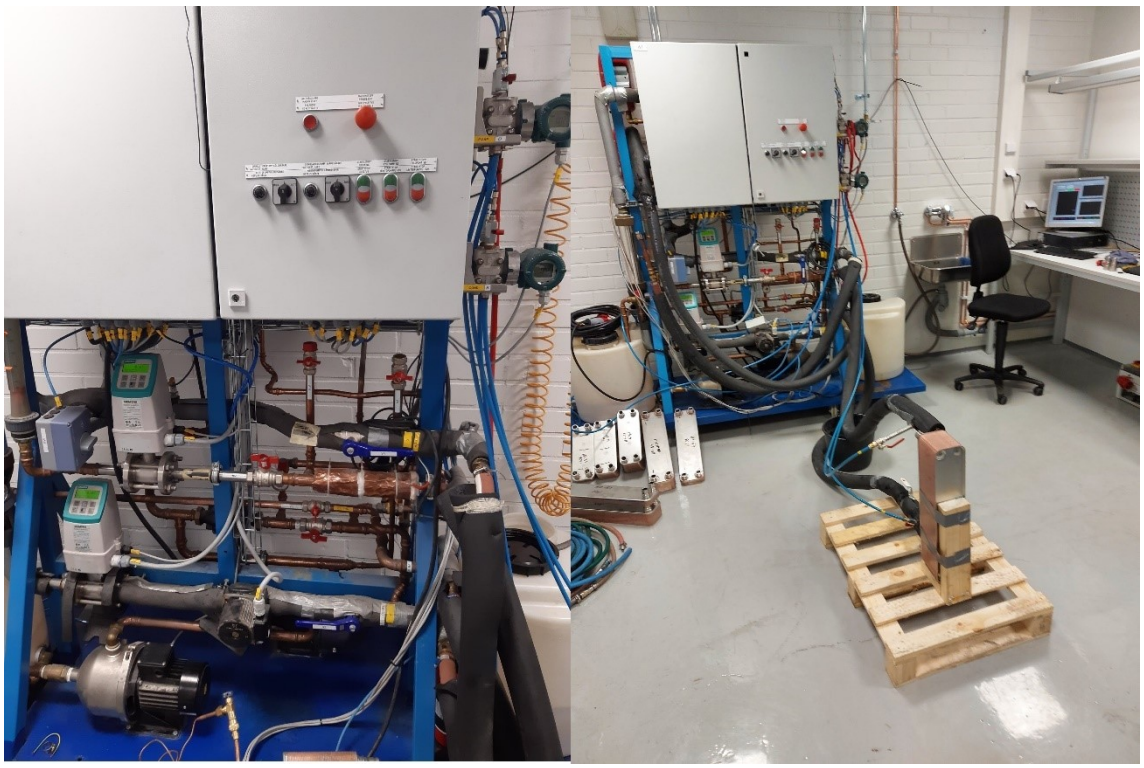

Figure 3.3. Setup used for pressure drop experiments.

3.2 Heat transfer data collection

3.2.1 Methodology

It is important that data are collected in the correct way in order to ensure that the model being built will function properly. As discussed in chapter 2.8.3, it can be difficult to distinguish the influences of different variables when studying the observed change in the overall heat transfer coefficient in different setups. The value of U can be modeled as a function dependent on the following variables:

$$U = f(\mathrm{Re}_h, \mathrm{Pr}_h, \mathrm{Re}_c, \mathrm{Pr}_c \dots) \tag{47}$$

Here the subscripts h and c stand for the hot and the cold stream. By varying the inlet temperatures and the volume flows for both streams, one can induce changes in the Reynold and Prandtl numbers. However, it is important to note that a change in any one of the inlet temperatures or volume flows will change the value of all the variables in equation (47). In order to ensure that the values for Re_h, Pr_h, and Pr_c stay relatively constant while Re_c is allowed to vary, the following methodology could be used.

An initial experimental run will be conducted for a specific heat exchanger with a given volume flow $\dot{V}_h$, a significantly smaller volume flow $\dot{V}_c$, and set inlet temperatures $T_{h,\,in}$ and $T_{c,\,in}$. The outlet temperatures are then measured, and the mean temperatures for the hot side $T_{h,\,\mathrm{m}}$ and the cold side $T_{c,\,m}$ are calculated.

For the second experiment, $\dot{V}_c$ will be increased slightly. This will lower the outlet temperature on the cold side, and the increased heat transfer will result in a slightly lower temperature in the hot side's outlet. Afterwards, the inlet temperatures $T_{h,\,in}$ and $T_{c,\,in}$ must be varied until the mean temperatures $T_{h,\,\mathrm{m}}$ and $T_{c,\,m}$ are the same as in the initial experiment. This way the values for Pr_h, and Pr_c remain constant, and as $\dot{V}_h$ was not changed, Re_h will also remain unchanged. Thus, the observed change in U between experiments can be attributed entirely to the change in Re_c. This procedure can then be repeated until enough data have been gathered.

The aforementioned methodology would in theory provide high-quality data, but the desired results with next to no deviations in the Prandtl numbers can be difficult to achieve in practice. Fernández-Seara et al. conducted experiments for demonstration purposes, and did not put significant effort into ensuring that the Prandtl number stayed exactly constant between experimental runs (Fernández-Seara et al., 2007, pp. 131–133). The parameters they obtained with the Wilson plot method proved to be satisfactory either way, as long as the Prandtl number stayed relatively constant (Fernández-Seara et al., 2007, p. 134).

3.2.2 Planned experiments

Experimental data are needed for each heat exchanger model that is to be included in the software. In theory, a single set of experiments with a specific number of plates ought to be sufficient to develop a method for predicting the heat transfer in that specific heat exchanger with any number of plates. In practice, however, experiments with different numbers of plates will be conducted in an effort to reduce the impact that measurement errors have on the final model. These experiments with different numbers of plates should yield the same parameter values C, m, and n when performing the Wilson plot method and is, as such, in and of itself a way to verify that the method works.

Table 3.1 lays out the experiments that are to be conducted with the 30-plate version of the heat exchanger HP-52B. As described in chapter 3.1, the volume flow for

one fluid is changed between experiments, in this case the hot side, in order to induce a change in the Reynold number. The inlet temperatures will be adjusted as necessary in order to maintain a constant mean temperature. $T_{h,\ out}$ and $T_{c,\ out}$ are measured with temperature sensors, and from there $\dot{Q}$ and ΔT_m can be calculated with equations (1) and (3). U is then calculated with equation (2), and Pr as well as Re are calculated for both sides with equations (14) and (15) respectively. A similar set of experiments are then conducted for the same heat exchanger with 60 plates, which can be seen in table 3.2.

Table 3.1. Planned experiments for HP-52B with 30 plates

Exchanger model	HP-52B
Number of plates	30

Experiment	T hot in	T hot out	T cold in	T cold out	V hot	V cold	LMTD	U	Heat Flux
#	°C	°C	°C	°C	l/h	l/h	°C	kW/m2K	kW
1	50		20		300	800			
2					450	800			
3					700	800			
4					850	800			
5					1000	800			
6					1150	800			
7					1300	800			
8					1450	800			
9					1600	800			
10					1750	800			

Table 3.2. Planned experiments for HP-52B with 60 plates

Exchanger model	HP-52B
Number of plates	60

Experiment	T hot in	T hot out	T cold in	T cold out	V hot	V cold	LMTD	U	Heat Flux
#	°C	°C	°C	°C	l/h	l/h	°C	kW/m2K	kW
1	50		20		400	1000			
2					600	1000			
3					800	1000			
4					1000	1000			
5					1200	1000			
6					1400	1000			
7					1600	1000			
8					1800	1000			
9					2000	1000			
10					2200	1000			

3.3 Pressure drop data collection

Data regarding the pressure drop will also be collected in order to verify the accuracy of equation (34). These tests will be performed separately on the same heat exchangers that are used in the heat transfer experiments. Here it is sufficient to only pump water through one side of the heat exchanger, as long as one knows how many channels that side has. This has the added benefit of keeping the temperature constant, making the analysis easier. Table 3.3 illustrates the experimental plan for the heat exchanger HP-64 with 30 plates.

Table 3.3. Planned pressure drop experiments for HP-64 with 30 plates

Exchanger model	HP-64
Number of plates	30

Experiment	T in	T out	Volume flow	Pressure drop
#	°C	°C	l/h	kPa
1	20	20	250	
2	20	20	500	
3	20	20	750	
4	20	20	1000	
5	20	20	1250	
6	20	20	1500	
7	20	20	1750	
8	20	20	2000	
9	20	20	2250	
10	20	20	2500	

4 Results and analysis

4.1 Experimental results

A table of all the experiments performed on each heat exchanger is presented in appendix A. Most of the data will be used in the construction of the calculation tool, with the exception of the heat transfer experiments performed on the 60-plate version of HP-64. Analysis suggests that this heat exchanger performed considerably below expectations in terms of heat transfer, and the inclusion of these datapoints would thus risk distorting the model. Possible explanations for this underperformance is discussed in chapter 4.2.2.

All experiments were performed with liquid water, as the setup did not allow for other fluids to be used. The Reynold number for all the experiments used in the construction of software model ranges between 100 and 1500, and the Prandtl number ranges between 4.7 and 6.3.

4.2 Determining Nusselt equation parameters

4.2.1 Wilson plot method

The modified Wilson plot method described in chapter 2.8.2 requires an iterative procedure in order to determine the exponent m, which would be time consuming to perform by hand. A MATLAB script that is included in appendix B is instead used to perform the calculations.

Here the Wilson plot method is applied to data gathered with a 30-plate version of the HP-52B exchanger, which is found in appendix A. The Prandtl exponent n is assumed to be 0.33, and an initial m value is estimated to be 0.7. As described in chapter 2.8, the overall thermal resistance R_{ov} is then plotted against $1/\mathrm{Re}^m$, and a straight line is fitted using linear regression. Figure 4.1 depicts this line alongside the coordinates for the individual points. Values for the constants C_1, C_2, and C are determined to be the following using equation (45):

$$\begin{cases} C_1 = 0.00003458 \\ C_2 = 0.01219 \\ C = 0.1180 \end{cases}$$

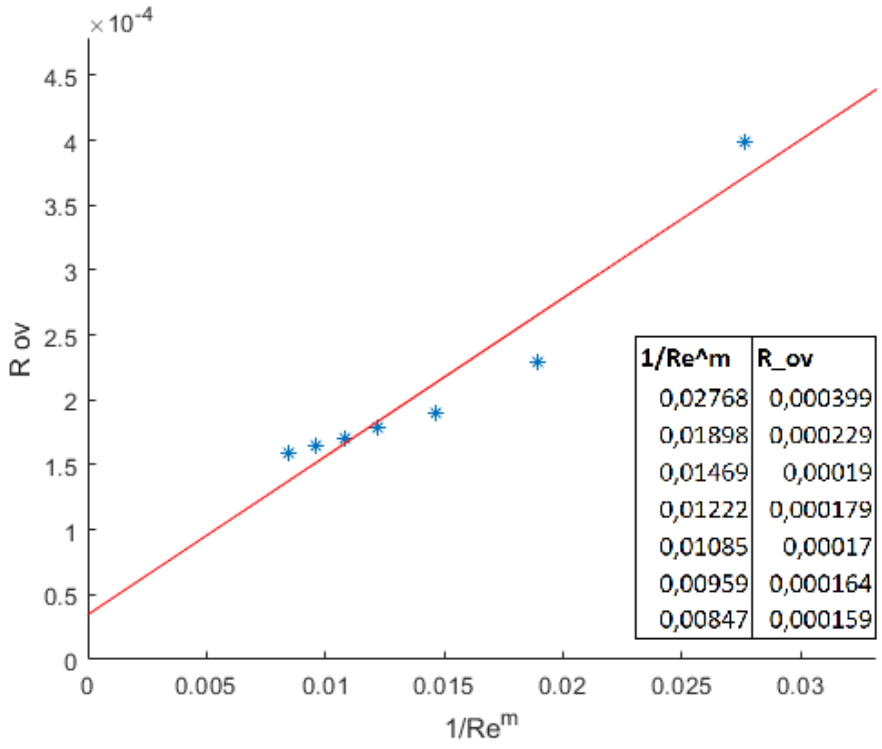

Figure 4.1. Plot of R_{ov} vs. $1/\mathrm{Re}^{m}$ for experiments using a 30-plate version of the HP-52B exchanger with $m = 0.7$.

Afterwards, $\ln[1/(R_{ov} - C_1)]$ is plotted against $\ln(\mathrm{Re})$ in accordance with the modified Wilson plot described in chapter 2.8.2 in order to determine the exponent m from the slope of the plot fitted line. Figure 4.2 depicts these datapoints alongside the plot fitted line.

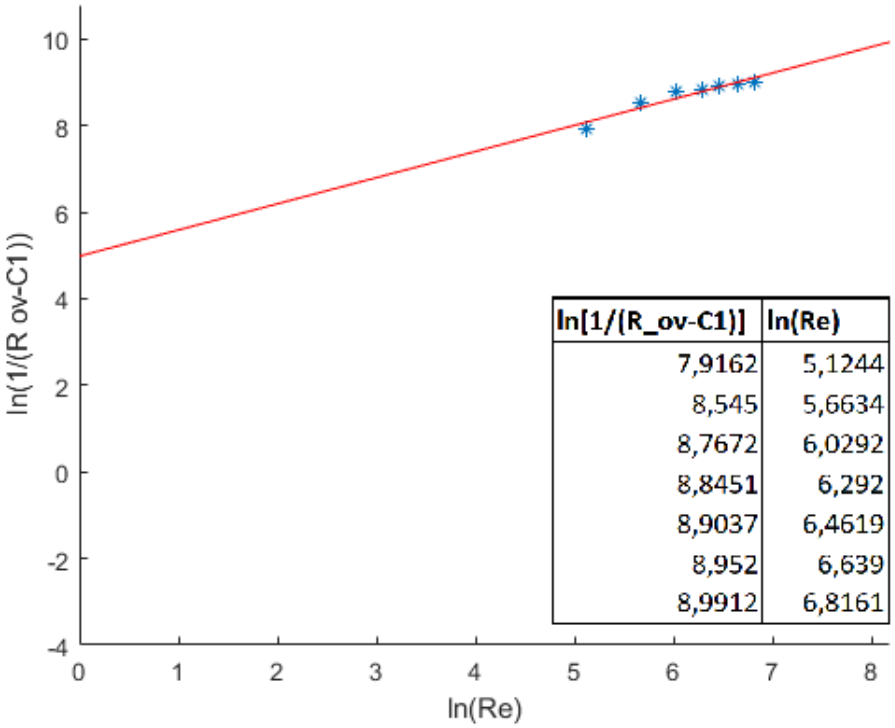

ln[1/(R_ov-C1)]	ln(Re)
7,9162	5,1244
8,545	5,6634
8,7672	6,0292
8,8451	6,292
8,9037	6,4619
8,952	6,639
8,9912	6,8161

Figure 4.2. Plot of ln(1/($R_{ov} - C_1$)) vs. ln(Re) for experiments using a 30-plate version of the HP-52B exchanger with C_1 = 0.00003458.

The slope of the line is determined to be 0.605, which differs substantially from the initial estimate of 0.7. From here on, the MATLAB script in appendix B is used to generate a new estimate for *m* and perform these calculations in an iterative fashion until the initial estimate coincides with the slope of the line in Figure X2. The result of this method is that the exponent *m* is estimated to be 2.034, and *C* is estimated to be 0.0001737. The corresponding plots are presented in Figure 4.3.

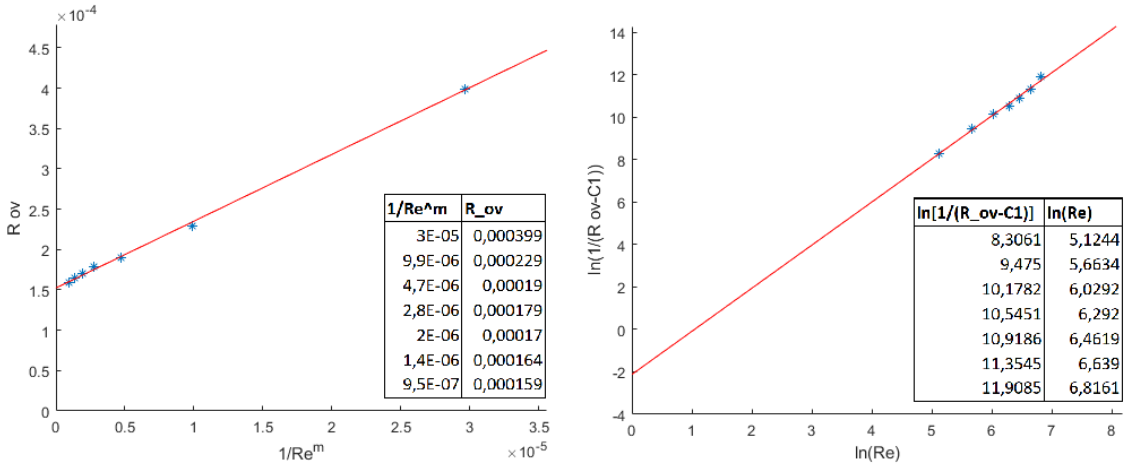

Figure 4.3. Wilson method plots for experiments using a 30-plate version of the HP-52B exchanger and an iterative MATLAB script with $m = 2.034$ and $C_1 = 0.0001523$.

It can be noted that plot fitted lines fit the data extremely well, but the estimated values for m and C are unrealistic and fail to yield accurate predictions regarding the heat exchangers performance when plugged into equation (37). Similar results are observed when the method is applied to experimental data for the heat exchangers HP-33 and HP-64.

One explanation for these results might be that the flows are laminar at the conditions tested, and the Wilson plot method works best with turbulent flows. This might not fully explain the results, as turbulence is expected to begin occurring at Re = 400 in plate heat exchangers with $\beta = 60°$ (Gherasim et al., 2011, p. 1501).

4.2.2 Alternative method

Another way to determine suitable parameters for equation (37) is to perform the heat transfer calculations with the data used in the experiments and predict the heat transfer area needed with all reasonable parameter combinations and then compare the outputs with the actual number of plates used. In practice, this is done by giving the same input data to the software model that were used in the experiments along with values for the parameters C and m. The model will then estimate the number of plates needed, and the results are compared to an answer sheet containing the actual number of plates used in the experiments. These parameters C and m are then stored as the "best" estimates, until a different combination yields predictions that deviate as little as possible from the experimental results. Figure 4.4 illustrates an algorithm written in pseudocode that will

perform the previously described task. Ideally separate parameters for laminar and turbulent flows should be developed, but the available dataset might be too small to justify fitting four parameters per heat exchanger.

```
for m in range (0.3 to 1.0)
    for C in range (0.1 to 0.5)

        ###
        Perform calculations using the inputs from experiments
        and the parameters C and m
        ###

        ###Store the predicted number of plates in an array
        model_predictions[]

        ###Compare the prediction to experimental results
        difference[] = experimental_results[] - model_predictions[]

        ###If this parameter combination yiels the best prediction thus far
        if difference[] < previous_best_difference[]

            ###Store the parameters values that yielded the best prediction
            m_best_guess = m
            C_best_guess = C
            previous_best_difference[] = difference[]
```

Figure 4.4. Pseudocode for determining the best Nusselt correlation parameters.

Roughly fifteen experiments per heat exchanger model covering a wide range of volume flows and sizes were used in determining the parameters. In the end, the following values were found to result in the best estimates.

$$HP-52B \begin{cases} C = 0.278 \\ m = 0.670 \end{cases}$$

$$HP-64 \begin{cases} C = 0.611 \\ m = 0.574 \end{cases} \quad (48)$$

$$HP-33 \begin{cases} C = 0.263 \\ m = 0.686 \end{cases}$$

It can be noted that the parameters for model HP-64 differ substantially from the other two models. The reason for this is difficult to attain, as it might be the result of a number of factors combined. One possible explanation is that the fluid does not flow in a uniform fashion for the relatively low volume flows tested, resulting in suboptimal heat transfer. This effect might be more prominent in the HP-64 model, as it is the biggest heat

exchanger tested, with the largest hydraulic diameter in the individual channels. Figure 4.5 shows infrared images of 60-plate versions of HP-52B and HP-64 in use, with a volume flow of about 1000 l/h in both the hot and the cold side. The images are taken with a Flir E40bx thermal camera.

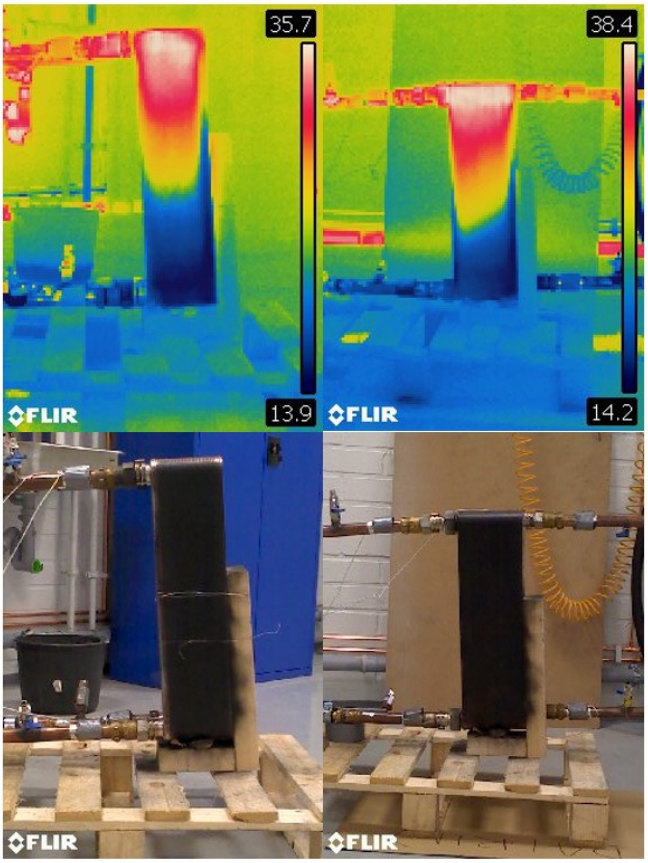

Figure 4.5. Infrared images of the heat exchangers HP-52B and HP-64 with 60 plates in use.

The thermal images clearly show that the channel velocity is not uniform at the volume flows tested for HP-64, compared to HP-52B. The fact that the theoretical model for the Nusselt number in equation (13) underestimates the number of plates needed to achieve the heat exchange in the experiments further suggests that the heat transfer at the volume flows tested is suboptimal, about 15% less than expected. A table comparing the model predictions is presented in chapter 4.4.

Any number of parameters could theoretically be fitted to the Nusselt number correlation using the previously described method, potentially leading to better predictions. A larger dataset would then be necessary to accommodate for this.

4.3 Pressure drop correction factor

Table 4.1 displays the measured pressure drop in the secondary channel for all the experiments performed with the HP-52B heat exchanger, as well as the predicted pressure drop using Zhu and Haglind's friction factor estimate (Zhu and Haglind, 2020, p. 9) presented in equation (30).

Table 4.1. Experimentally measured pressure drop and theoretically predicted pressure drop for experiments performed with the HP-52B heat exchanger.

HP-52B Target flowrate (l/h)	250	500	750	1000	1250	1500	1750	2000	2250	2500	2750
10pl											
flow (l/h)	249,563	498,948	749,5125	999,289	1247,93						
measured pdrop (kPa)	3,42292	12,0879	25,4935	43,4537	65,7471						
calculated pdrop (kPa)		9,7	21,1	36,79	56,75						
correction factor		1,246	1,208	1,181	1,159						
30pl											
flow (l/h)	250,13	499,896	749,934783	1000,09	1249,71	1500,09	1749,84	2000,18	2249,66		
pressure drop (kpa)	0,57261	1,86667	3,90391304	6,4984	9,89167	13,7952	18,1971	23,1239	28,535		
calculated kPa		1,36	2,79	4,71	7,14	10,07	13,5	17,43	21,86		
correction factor		1,373	1,399	1,38	1,385	1,37	1,348	1,327	1,305		
60pl											
flow (l/h)	249,913	499,896	749,96875	999,815	1250,39	1499,79	1749,95	1999,92	2249,51	2498,8	2572,94
pressure drop (kpa)	0,22261	0,62167	1,2575	2,10652	3,13167	4,34583	5,74	7,29958	9,03913	10,9363	11,5292
calculated kPa		0,47	0,91	1,48	2,2	3,06	4,06	5,2	6,48	7,9	8,35
correction factor		1,323	1,382	1,423	1,423	1,42	1,414	1,404	1,395	1,384	1,381

Figure 4.6 contains the pressure drop experimental results for HP-52B with 30 plates, as well as theoretical estimates using equation (34) with Martin's friction factor estimate (27) as well as Zhu and Haglind's estimate (30). Both models underestimate the pressure drop, but Zhu and Haglind's estimate seems to be off by a constant factor. Similar results can be observed in the other experiments. In this case, the theoretical estimate is off by a factor of roughly 1.36 on average. A good correlation is achieved by introducing this correction factor, as can be seen in Figure 4.6. One plausible explanation for this mismatch between the theoretical predictions and the observed results might be

that the friction factor in the heat exchanger is underestimated at all volume flows. Another explanation could be that equation (34) underestimates the pressure drops in the inlet and outlet ports. This could have been tested by performing experiments on the same heat exchangers with differently sized ports. A closer analysis of the current data might also give some better insight into the inlet and outlet effects, as most heat exchangers tested used the same ports.

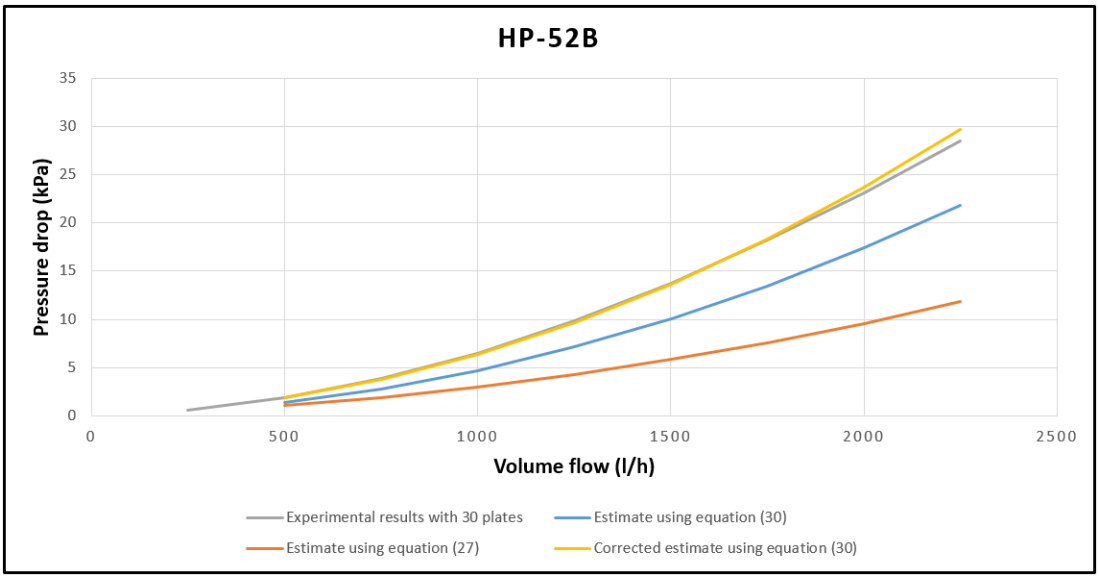

Figure 4.6. Experimental results and theoretical predictions for the pressure drop in an HP-52B heat exchanger with 30 plates.

Setting a constant correction factor can, however, be quite limiting, as experiments presented in table 4.1 show that different numbers of plates and different volume flows demand different correction factors. One solution is to calculate how much the theoretical prediction is off from each experiment, which is included in table 4.1, and then use these numbers to construct a two-variable function that predicts the correction factor for a given number of plates and volume flow. Using the curve fitting tool in MATLAB with the volume flow and number of plates as independent variables, the following polynomial was fitted for the heat exchanger HP-52B:

$$c_{f,HP-52B}(n_p, \dot{V}) = 1.08 - 5.16 \cdot 10^{-8}\dot{V}^2 + 4.49 \cdot 10^{-6}\dot{V} - 1.96 \cdot 10^{-4}{n_p}^2$$

$$+1.51 \cdot 10^{-2}n_p + 2.75 \cdot 10^{-6}\dot{V}n_p \qquad (49)$$

This function is illustrated graphically in Figure 4.7. It has a coefficient of determination R^2 = 0.966, indicating a good fit. The predictive power outside the scope of the

experiments, that is for heat exchangers with over 60 plates is probably unreliable and, thus, the correction factor for these cases is assumed to be equal to the correction factor with 60 plates. Similar equations were constructed for the heat exchangers HP-33 and HP-64 and can be found in equations (50) and (51).

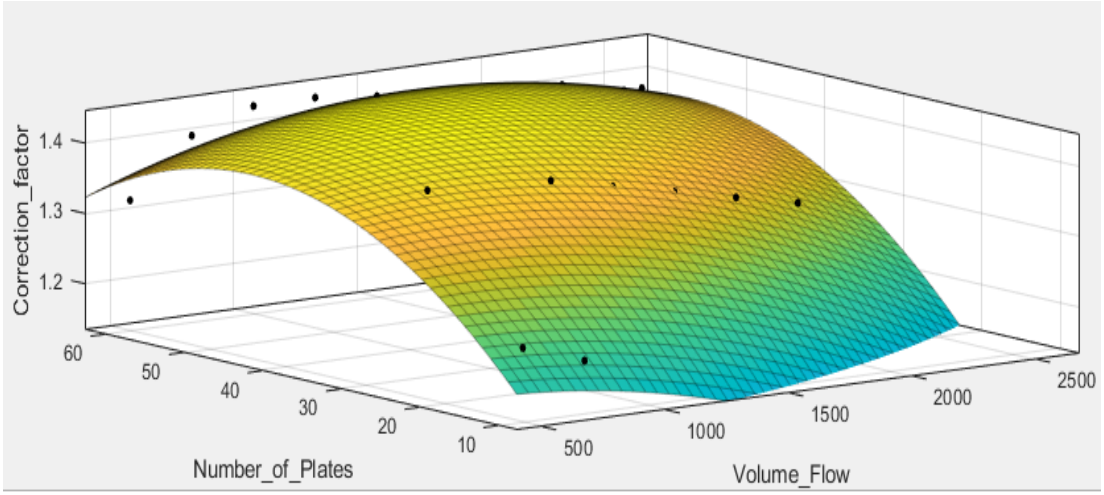

Figure 4.7. Graphical depiction of equation (49). The black dots are the correction factors for individual experiments in Table 4.1.

$$c_{f,HP-33}(n_p, \dot{V}) = 1.34 + 5.02 \cdot 10^{-11}\dot{V}^3 - 2.64 \cdot 10^{-7}\dot{V}^2 + 3.89 \cdot 10^{-6}\dot{V}$$
$$+4.70 \cdot 10^{-5}{n_p}^2 - 7.63 \cdot 10^{-3}n_p - 3.03 \cdot 10^{-10}\dot{V}^2 n_p - 1.79 \cdot 10^{-7}\dot{V}\,{n_p}^2$$
$$+1.89 \cdot 10^{-5}\dot{V}\,n_p \quad (50)$$

$$c_{f,HP-64}(n_p, \dot{V}) = 1.57 - 3.58 \cdot 10^{-8}\dot{V}^2 - 3.70 \cdot 10^{-5}\dot{V} - 1.89 \cdot 10^{-4}{n_p}^2$$
$$+5.42 \cdot 10^{-3}n_p + 3.12 \cdot 10^{-6}\dot{V}n_p \quad (51)$$

The correction factor for HP-33 was fitted to a third-degree polynomial, resulting in a coefficient of determination R^2 = 0.943. A second-degree polynomial only resulted in R^2 = 0.742, indicating a relatively poor fit. The correction factor for HP-64 has a coefficient of determination R^2 = 0.969.

4.4 Model verification

The constructed model's ability to predict the performance of the included heat exchangers is verified by comparing the estimated heat transfer and pressure drop for a given input with the data gathered from experiments. Additional data gathered during previous test runs that were not included in the construction of the model are also included in the comparison in order to ensure that the model performs adequately outside the scope of the data used to build it.

The capabilities to determine the heat transfer between fluids other than water could not be verified for the different models, as no such test data was available for comparison.

4.4.1 Heat transfer

Table 4.2 contains a comparison of the heat transfer experimental results, theoretical performance predictions, and the constructed model's predictions. Here data about inlet and outlet temperatures, as well as volume flows, are taken from experiments found in Appendix A, and are given as inputs to the software models. The number in the first column denotes which experimental values are being used, with the exception of the last two experiments in the HP-64 column, which are taken from a different dataset. The models then predict the number of plates needed to facilitate the heat exchange, and the result is compared to the known number of plates used in the experiment. The column "Martin Model" contains predictions using Martin's Nusselt correlation presented in equation (13), as well as his friction factor estimate in equation (27). The column "Dović et al" contains predictions using equations (17) through (24), which are constructed by modeling the heat transfer in individual sine sections. The "Experimental Model" column uses the generalized Nusselt equation (37) with heat exchanger specific parameters from (48) and $n = 0.33$. The viscosity correction factor has been left out, as it is difficult to predict the internal wall temperatures across the heat exchanger, and as the factor has a miniscule impact on the result anyway. Assuming a temperature difference of 3° C between the wall and the fluid, the correction factor is roughly 1.015 for water, which is likely to be overshadowed by errors in other estimates. This factor will also be offset to a certain degree by the affected heat transfer on the other side of the wall.

Table 4.2. Comparison between the number of plates used in experiments and the model's predicted number of plates needed to facilitate the given heat transfer.

HP-52B	Answer	Martin Model	Dovic et al Model	Experimental Model
10pl				
2	10	6	0	6
3	10	6	0	6
4	10	6	0	4
5	10	6	0	6
6	10	6	0	6
30pl				
2	30	30	28	30
3	30	36	34	36
4	30	34	32	34
5	30	36	34	34
6	30	36	32	36
7	30	34	30	32
60pl				
2	60	38	34	38
3	60	46	44	48
4	60	48	48	52

HP-33	Answer	Martin Model	Dovic et al Model	Experimental Model
10pl				
3	10	10	0	8
4	10	10	0	8
5	10	10	0	8
6	10	10	0	8
7	10	6	0	6
30pl				
1	30	28	22	28
2	30	34	26	30
3	30	36	26	32
4	30	38	28	34
5	30	36	26	32
6	30	34	24	30
60pl				
1	60	40	34	42
2	60	54	46	56
3	60	60	50	60
4	60	46	44	52

HP-64	Answer	Martin Model	Dovic et al Model	Experimental Model
10pl				
2	10	8	0	6
3	10	10	0	6
4	10	8	0	6
5	10	10	0	8
6	10	10	0	8
30pl				
2	30	34	26	20
3	30	42	34	26
4	30	48	40	28
5	30	48	40	30
52pl				
1	52	92	82	54
2	52	104	86	62

It can be noted that the theoretical model makes surprisingly good predictions, especially for the smallest heat exchanger, HP-33. This might in part be due to the reasons discussed in chapter 4.2.2, meaning that the fluid flows are more developed in small channels at relatively low flowrates. The experimental model using individual parameters for each heat exchanger performs slightly better in heat exchangers with more plates, and the difference is especially apparent in large versions of HP-64.

The model developed by Dović et al. failed to yield any outputs for 10-plate versions of any heat exchanger. This model had the largest Nusselt number estimates in general, and as such predicts the fewest number of plates. The calculation tool had difficulties with plate estimates under six, and this probably why the model did not work.

4.4.2 Pressure drop

Table 4.3 presents a comparison between the experimentally measured pressure drop, and the model's corrected theoretical predictions for experiments performed with HP-52B. This corrected prediction is constructed by multiplying the theoretically calculated pressure drop using equations (34) and (30), with the correction factor for HP-52B presented in equation (49).

Table 4.3. Experimentally measured pressure drop for HP-52B, and the model's predicted pressure drop.

HP-52B Target flowrate (l/h)	250	500	750	1000	1250	1500	1750	2000	2250	2500	2750
10pl											
Flow (l/h)	249,563	498,94792	749,5125	999,289	1247,93						
Measured pdrop (kPa)	3,42292	12,087917	25,4935	43,4537	65,7471						
Estimated pdrop (kPa)		11,8	25,49	43,92	66						
Overestimate (%)		-2,4	0	1,1	0,4						
30pl											
Flow (l/h)	250,13	499,89583	749,934783	1000,09	1249,71	1500,09	1749,84	2000,18	2249,66		
Measured pdrop (kPa)	0,57261	1,8666667	3,90391304	6,4984	9,89167	13,7952	18,1971	23,1239	28,535		
Estimated pdrop (kPa)		1,89	3,89	6,57	9,9	13,83	18,28	23,15	28,31		
Overestimate (%)		1,2	-0,4	1,1	0,1	0,3	0,5	0,1	-0,8		
60pl											
Flow (l/h)	249,913	499,89583	749,96875	999,815	1250,39	1499,79	1749,95	1999,92	2249,51	2498,8	2572,94
Measured pdrop (kPa)	0,22261	0,6216667	1,2575	2,10652	3,13167	4,34583	5,74	7,29958	9,03913	10,9363	11,5292
Estimated pdrop (kPa)		0,63	1,25	2,08	3,11	4,35	5,77	7,36	9,1	10,94	11,5
Overestimate (%)		1,3	-0,6	-1,3	-0,7	0,1	0,5	0,8	0,7	0	-0,3

For this specific heat exchanger, the largest divergence between the experimental results and the theoretical predictions is just 2.4%, and for most experiments the prediction is within 1% of the actual pressure drop.

The estimated pressure drops at 250 l/h were left out, as the calculation tool had trouble when very low volume flows were given as inputs.

5 Calculation tool development

Loval currently has access to a calculation tool built in Excel that uses equations and estimates from a previous thesis work.

The biggest drawback to building a calculation tool in Excel is the difficulty of designing an intuitive interface, and as such there is a risk of creating a poor user experience. It will be difficult for the user to utilize the tool at an advanced level without at least some insight into how the model functions and what the individual cells do. The user might also grow frustrated as a lot of redundant information tends to be displayed, and as a result the tool risks falling out of use.

It was decided early on that a proper standalone piece of software would be developed in order to meet the demands of delivering a functional user experience. The software will be written in Python as that is the language the author is most familiar with, and the Python toolkit Qt will be used to implement the graphical user interface.

5.1 Frontend

When designing a graphical user interface, the user experience must always be the prime focus. The user should easily be able to identify where inputs are required, and what buttons to press to perform certain actions.

Figure 5.1 depicts the final version of the GUI. It contains the ability for the user to input data regarding the primary and secondary streams, and the total heat flux. The program calculates the value for any cell that is left empty, the LMTD, and the total number of plates needed. In order not to overwhelm the user with information, additional calculation outputs like flow velocities and different dimensionless numbers are presented under a different tab labeled "Details". The software includes features like the ability to switch between different fluids and heat exchangers designs with different parameters.

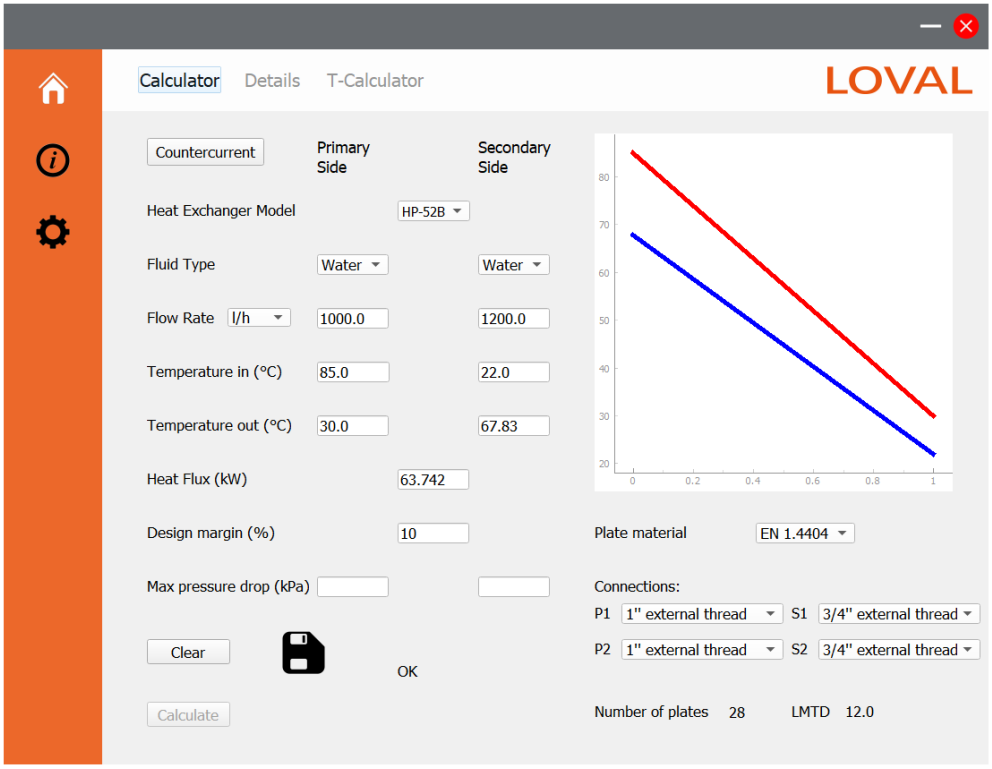

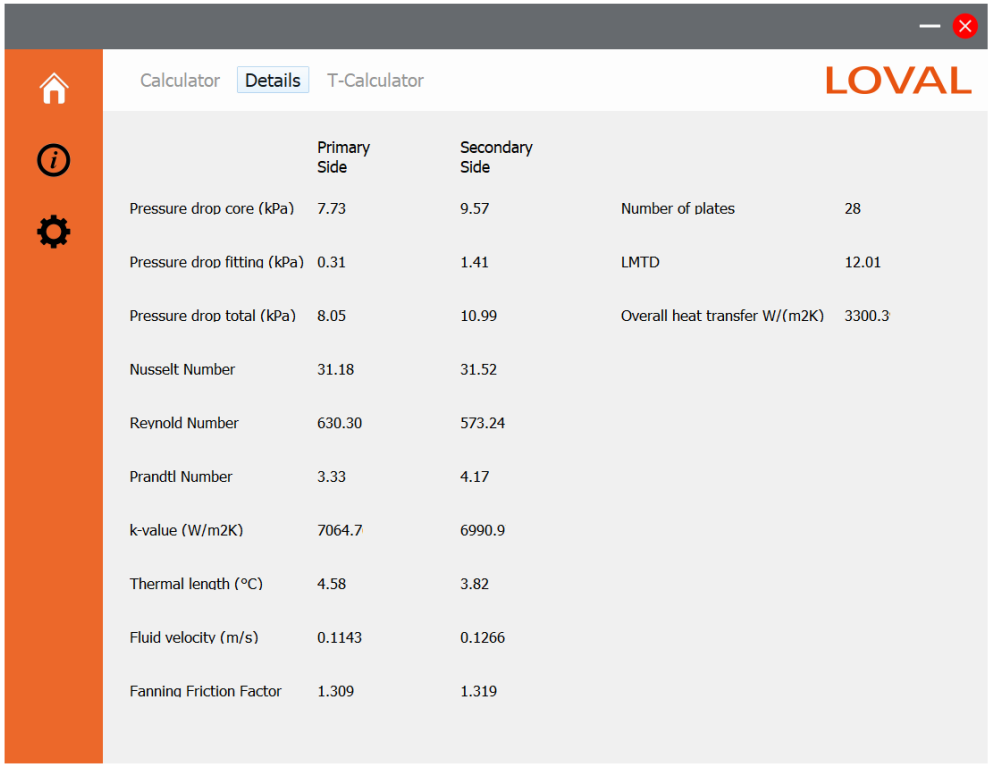

Figure 5.1. The calculation tool's graphical user interface

In practice, heat exchangers are often slightly over dimensioned compared to the theoretical estimate. One reason can be in order to ensure that they perform adequately in cases where fouling is a factor, which would reduce the heat transfer performance. Thus, the ability to set a design margin percentage was implemented.

The user can also set a maximum allowed pressure drop which the software takes into account, adding additional plates as necessary in order to lower the flow rate inside the core. Different plate materials and connection sizes are also available to choose from.

One requested feature was the ability to save the results of a calculation in a presentable document, preferably in a PDF format. This document could be used just as an internal reference, or it could potentially be sent to customers as an estimate of what to expect. In the software, this function is implemented as a single button press that becomes enabled once the calculate button has been pressed and a feasible solution has been found.

Finally, a method for the user to add additional heat exchanger models with unique parameters was requested. This feature could be implemented as a button in the GUI where the user is asked to input a name for the heat exchanger along with parameter values. This would, however, be tedious work, as such a feature would also necessitate a way to make changes to already existing heat exchangers, as well as a way to delete them. It was therefore decided that new heat exchangers will be added by modifying an accompanying text file. While this solution might not be particularly user friendly, it saves a lot of work on the programmer's side. Figure 5.2 depicts the text file containing one heat exchanger with hypothetical parameter values.

```
def exchanger_model == "HP-90":
        Steel_therm_cond = 16.3                 #W/mK
        Plate_thickness = 0.0005                #m
        Plate_width = 0.15                      #m
        Plate_width_fitting = 0.14              #m
        Plate_length = 0.5                      #m
        Plate_length_fitting = 0.47             #m
        Wave_height = 0.002                     #m
        Wave_length = 0.004                     #m
        Chevron_angle = 50                      #degrees
        Fitting_diameter = 0.024                #m
        m = 0                                   #Parameter for Nusselt equation
        C = 0                                   #Parameter for Nusselt equation
        use_theoretical_model = True            #True/False
        Thickness = N_plates*2.3+17             #mm
        Weight = N_plates*0.23+2.6              #kg
```

Figure 5.2. Hypothetical heat exchanger added to the accompanying text file.

5.2 Backend

Backend refers to the "behind the scenes" functionality of the software and contains all the algorithms and methods needed to transform user input into outputs.

5.2.1 Heat transfer area

A simplified version of the central algorithm used to estimate the number of plates needed to facilitate a specific heat transfer is illustrated in Figure 5.3. The user is initially asked to give five inputs out of the following seven: $\dot{Q}$, $\dot{V}_h$, $\dot{V}_c$, $T_{h,\,in}$, $T_{h,\,out}$, $T_{c,\,in}$, $T_{c,\,out}$. The remaining two values are then calculated with equation (1). Afterwards, the following equation can be constructed by combining equations (2) and (11), and substituting the total area A for area per plate A_p times the number of plates n_p:

$$\frac{\dot{Q}}{A_p n_p \, \Delta T_m} = \left(\frac{1}{\alpha_h} + \frac{\delta_P}{k_P} + \frac{1}{\alpha_c} + R_{f,h} + R_{f,c}\right)^{-1} \tag{52}$$

Here the convective heat transfer coefficients α_h and α_c can further be expanded as follows:

$$\alpha = \frac{kC\left(\frac{\rho\left(\frac{\dot{V}}{A_c n_c}\right) D_H}{\mu}\right)^m \left(\frac{c_p \mu}{k}\right)^n}{D_H} \tag{53}$$

where

$$\begin{cases} n_c = \dfrac{n_p}{2} - 1 & \text{for primary side} \\ n_c = \dfrac{n_p}{2} & \text{for secondary side} \end{cases} \tag{54}$$

Here C, m, and n are the parameters that have been calculated to fit equation (37). Each heat exchanger model has separate values for these parameters. From here on, the only unknown in equation (52) is the number of plates n_p. A numerical method is then used in the algorithm to solve for n_p, as it might be impossible to solve analytically.

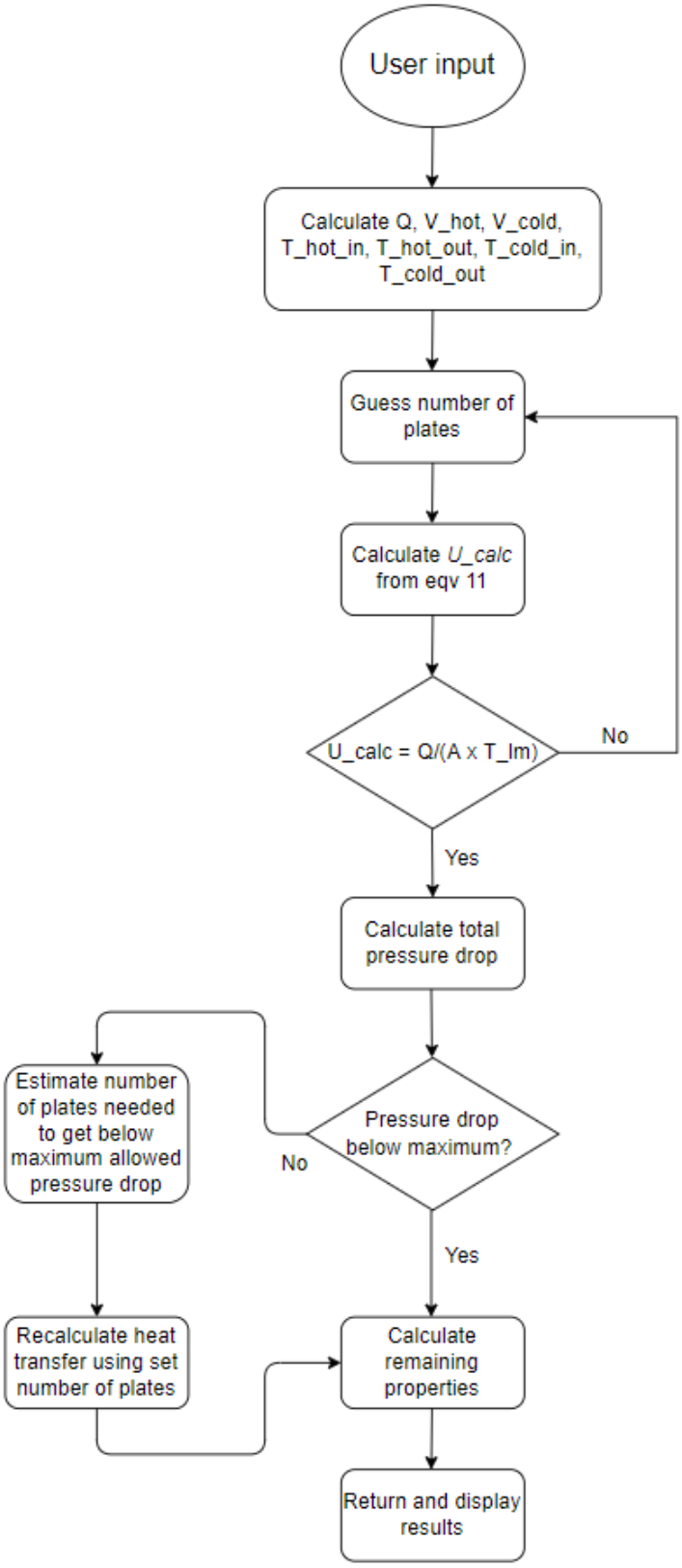

Figure 5.3. Simplified flowchart of the calculation tool's algorithm

5.2.2 Pressure drop

Once the total number of plates needed is known, additional information is calculated, such as the total pressure drop using equations (34), (35), and (36), as well as the physical properties of the heat exchanger, like the thickness and weight. Equation (34) needs an estimate of the friction factor, and as discussed in chapter 4.3, the estimate provided by Zhu and Haglind (Zhu and Haglind, 2020, p. 9) proved to consistently underestimate the pressure drop. The introduction of a simple correction factor results in predictions that match experimental data within 5% in virtually all cases.

$$\Delta p = \left(\frac{1.5 {G_p}^2}{2\rho_i} + \frac{2 f L_H G^2}{D_H \rho_m} + \left(\frac{1}{\rho_o} - \frac{1}{\rho_i} \right) G^2 \pm \rho_m g L_H \right) c_f \tag{55}$$

Here c_f is the heat exchanger specific correction factor from equations (49), (50), and (51), ranging in value from 1.2 to 1.5, depending on the heat exchanger model, the number of plates, and the volume flow $\dot{V}$.

If the previously calculated pressure drop exceeds the maximum allowed pressure drop defined by the user, the number of plates needs to be re-estimated. This can be done in an iterative fashion where two plates are added to the previous estimate and the pressure drop is recalculated. This is then repeated until the total pressure drop no longer exceeds the maximum allowed. Afterwards, the temperatures of the outgoing streams need to be recalculated, because the total heat transfer has increased as a result of the increased surface area. A separate algorithm described in chapter 5.2.3 is used for this task.

5.2.3 Total heat transfer estimate

Estimating the heat transfer that will occur in a heat exchanger with a given number of plates is done using the same equation (52) as when estimating the number of plates needed to facilitate a specific heat transfer. In this case, however, the temperatures at the outlets are unknown. These temperatures can be described by rearranging equation (1):

$$\begin{cases} T_{h,out} = T_{h,in} - \dfrac{\dot{Q}}{c_{p,h} \dot{m}_h} \\ \\ T_{c,out} = T_{c,in} + \dfrac{\dot{Q}}{c_{p,c} \dot{m}_c} \end{cases} \tag{56}$$

This leaves $\dot{Q}$ as the only unknown in equation (52), as ΔT_m can be determined by inserting equation (56) wherever necessary.

The method described in chapter 2.3.1 for determining a mean fluid parameter value between two temperatures is used throughout the software. If the outlet temperature is described with equation (56), the parameter equation would take the following form for the hot side:

$$\frac{1}{T_{h,in} - \left(T_{h,in} - \frac{\dot{Q}}{c_{p,h}\dot{m}_h}\right)} \int_{T_{h,in} - \frac{\dot{Q}}{c_{p,h}\dot{m}_h}}^{T_{h,in}} f_h(T)\, dT \tag{57}$$

Here $f_h(T)$ is a general function describing some fluid parameter such as viscosity or density as a function of temperature. This gives rise to a problem, as the numerical integrator used in the software only accepts numerical values as limits. This would not be a problem if $f_h(T)$ could be solved symbolically for all fluid properties, as the integral could be then solved as follows:

$$\left[F_h(T)\right]_{T_{h,in} - \frac{\dot{Q}}{c_{p,h}\dot{m}_h}}^{T_{h,in}} = F_h\left(T_{h,in}\right) - F_h\left(T_{h,in} - \frac{\dot{Q}}{c_{p,h}\dot{m}_h}\right) \tag{58}$$

Here $F_h(T)$ is the antiderivative of $f_h(T)$. Most fluid properties in the software tool are described using plot fitted polynomial functions and , as such, finding the antiderivative is trivial. Some functions, however, could not be solved symbolically, and equation (58) could thus not be used as a solution.

The implemented workaround consists of giving an initial estimated value to $\dot{Q}$ for the purpose of determining the fluid parameters with equation (57). Afterwards, $\dot{Q}$ is redefined as a variable, and equation (52) is solved. If the initial estimate and the calculated heat transfer differ from one another, new fluid parameters are estimated using the previously calculated heat transfer. The estimated and the calculated heat transfer values usually converge after two or three iterations, and the algorithm returns the outlet temperatures.

5.2.4 Design margin

The implementation of a design margin feature is easily achieved by altering equation (52) in the following way:

$$\left(1+\frac{x}{100}\right)\frac{\dot{Q}}{A_p n_p\,\Delta T_m}=\left(\frac{1}{\alpha_h}+\frac{\delta_P}{k_P}+\frac{1}{\alpha_c}+R_{f,h}+R_{f,c}\right)^{-1} \tag{59}$$

Here x is the design margin as a percentage. The estimated number of plates tends to increase rapidly for small increases in design margin, as the total heat transfer Q does not scale one to one with an increased number of plates. This is because while an increased number of plates leads to more heat transfer area, it also reduces the fluid velocity through the core, thereby resulting in a lower Reynold number, and as such, a lower Nusselt number.

5.2.5 Generating calculation reports

The open-source package ReportLab was used in order to generate PDF reports for calculations (ReportLab-Inc, 2021). The method takes all the results from a successful calculation as inputs, converts them into appropriate units, rounds them as necessary, and presents them at predetermined locations on an A4-sized document. It also attaches an illustrative Figure of a heat exchanger and prints the physical dimensions, including the thickness depending on the estimated number of plates needed as well as information regarding the connections used. An example of a generated report is available in Appendix C.

6 Summary and Conclusion

A calculation tool capable of predicting the thermodynamic performance of a number of brazed plate heat exchangers to a satisfactory degree was successfully developed for Loval Oy. This was achieved by developing a mathematical model of the expected heat transfer using Nusselt number estimates specific to each heat exchanger included in the software. A graphical user interface was developed to enhance the user experience, allowing for different plate heat exchanger designs, fluids, and connections to be used in the calculations.

Heat transfer and pressure drop experiments were performed in Loval's laboratory in Loviisa in order to construct a function for the Nusselt number, and to validate the software's calculations. Experiments with liquid water showed that a purely theoretical model yielded relatively good performance predictions for smaller heat exchangers, but severely underestimated the performance of the largest heat exchanger tested. The data gathered allowed for the construction of models specific to each heat exchanger, resulting in performance predictions that matched reality more closely. Experiments also showed that the theoretical model underestimated the pressure drop in all heat exchangers by 10-30% depending on the volume flow and number of plates, and as such a correction factor was introduced.

The reliability of the software's calculations could be further improved by finding and implementing a better Nusselt number estimate for chevron plate heat exchangers. Additional features that could be included but were deemed to be outside the scope of this work are the inclusions of evaporation and condensation as well as a web-based user interface for potential customers.

7 Summary in Swedish – Svensk sammanfattning

Dimensionering av plattvärmeväxlare är en tidskrävande och beräkningsintensiv process. Beräkningarna bör dock göras, eftersom kunder inte vill betala för en större värmeväxlare än nödvändigt, och vissa begränsande faktorer som tryckfallet måste kännas till. Målet med denna avhandling var att utveckla ett sådant beräkningsprogram för Loval Oy som tillåter användaren att snabbt och enkelt mata in data om en viss värmeöverföring, och därefter få ut dimensionerna på en värmeväxlare som klarar av uppgiften i fråga. I arbetet ingår förutom programvaruutvecklingen även en litteraturstudie för att fastställa vilka teoretiska ekvationer och formuleringar som lämpar sig som grund i beräkningsprogrammet. Dessutom utfördes experimentella test i Lovals laboratorium i Lovisa för att undersöka tillförlitligheten hos programmets beräkningar och introducera olika korrektionsfaktorer.

7.1 Teoretisk bakgrund

Den totala värmeenergin som överförs från ett varmare medium till ett kallare i en plattvärmeväxlare beskrivs i följande ekvation:

$$\dot{Q} = U\, A\, \Delta T_m \tag{2}$$

(Sekulić och Shah, 2003, s. 83)

Här är $\dot{Q}$ värmeöverföringen, U värmegenomgångstalet, A värmeöverföringsytans area, och ΔT_m den logaritmiska medeltemperaturskillnaden mellan fluiderna. U är beroende av värmeöverföringstalet α för båda fluiderna, vilket i sin tur är beroende av Nusselts tal enligt följande:

$$\alpha_i = \frac{k_i \mathrm{Nu}}{D_H} \tag{12}$$

Här är i mediet i fråga, k den termiska konduktiviteten och D_H den hydrauliska diametern. Nusselts tal är inom flödesdynamik ett dimensionslöst förhållande mellan den konvektiva och konduktiva värmeöverföringen. Litteraturstudien visade att det inte existerar någon allmänt accepterad metod för att uppskatta Nusselts tal i plattvärmeväxlare, främst för att små variationer i plattornas struktur kan innebära stora skillnader i

värmeöverföringsförmågan. I en litteraturstudie sammanfattade Zahid 26 olika artiklar som alla föreslog egna uppskattningar på Nusselts tal i plattvärmeväxlare (Zahid, 2003, s. 9–12).

En populär uppskattning av Nusselts tal för chevron plattvärmeväxlare som Loval producerar är Martins uppskattning från 1996.

$$\mathrm{Nu} = 0.205\mathrm{Pr}^{\frac{1}{3}}\left(\frac{\mu_m}{\mu_w}\right)^{\frac{1}{6}}\left(f\mathrm{Re}^2 sin(2\beta)\right)^{0.374} \tag{13}$$

(Sekulić och Shah, 2003, s. 515)

Här är Pr Prandtls tal, Re Reynolds tal, f Fanning friktionsfaktorn, β chevron vinkeln för värmeväxlarplattan och μ mediets dynamiska viskositet. Genom att kombinera alla tidigare nämnda ekvationer kunde en teoretisk modell konstrueras som klarar av att lösa värmeöverföringsproblemet med avseende på värmeöverföringsytan A, vilket ger en uppskattning på antalet plattor som behövs för en viss värmeväxlarmodell.

Tryckfallet i en plattvärmeväxlare kan uppskattas med följande ekvation:

$$\Delta p = \frac{1.5{G_p}^2}{2\rho_i} + \frac{2fL_H G^2}{D_H \rho_m} + \left(\frac{1}{\rho_o} - \frac{1}{\rho_i}\right) G^2 \pm \rho_m g L_H \tag{34}$$

(Sekulić och Shah, 2003, s. 397)

Här är L_H värmeväxlarplattans effektiva längd, D_H den hydrauliska diametern, ρ mediets densitet, och g tyngdkraftsaccelerationen. G och G_p betecknar massflödeshastigheten genom kärnan samt anslutningarna. Denna ekvations tillförlitlighet undersöktes experimentellt i Lovals laboratorium och en korrektionsfaktor introducerades.

7.2 Experimentell datainsamling

För att bättre kunna modellera specifikt Lovals plattvärmeväxlare, gjordes en separat uppskattning av Nusselts tal för varje värmeväxlare med en generaliserad version av Sieder-Tate-ekvationen som grund.

$$\mathrm{Nu} = C\mathrm{Re}^{m}\mathrm{Pr}^{n}\left(\frac{\mu}{\mu_w}\right)^{0.14} \tag{16}$$

(Sieder och Tate, 1936, s. 1429–1435)

Denna uppskattning gjordes genom att utföra experiment där värmeöverföringsförmågan hos olika värmeväxlarmodeller uppmättes. Tabell 7.1 innehåller de experiment som utfördes på värmeväxlaren HP-52B med 30 plattor. Andra värmeväxlare som inkluderades i testen var HP-33 och HP-64.

Tabell 7.1. Värmeöverföringsexperiment för HP-52B med 30 plattor.

Värmeväxlar modell	HP-52B
Antal plattor	30

Experiment	T varm in	T varm ut	T kall in	T kall ut	Flöde varm	Flöde kall	T medel v	T medel k	Re varm	Re kall	LMTD	U	Q
#	°C	°C	°C	°C	l/h	l/h	°C	°C			°C	kW/m2K	kW
1	44,87	21,78111	21,1344	30,11444	420	1077,458	33,32556	25,62444	168,0802	334,1035	4,511172	1,318092	11,22751
2	45,05417	19	17,085	34,87333	720	1052,201	32,02708	25,97917	288,1375	326,2718	4,947263	2,325025	21,71904
3	44,96111	18,86056	13,055	38,80889	1038	1049,611	31,91083	25,93194	415,3982	325,4688	5,977213	2,779273	31,36737
4	44,90368	22,44632	11,6705	41,65895	1350	1008,703	33,675	26,66474	540,2578	312,7837	6,274478	2,96277	35,10133
5	43,71056	24,42611	11,6733	41,40722	1600	1035,38	34,06833	26,54028	640,3055	321,0558	6,105817	3,098606	35,72383
6	42,92231	26,88231	11,8746	41,49154	1910	1032,101	34,90231	26,68308	764,3647	320,039	5,776552	3,252011	35,47061
7	41,345	28,88125	12,1106	40,52313	2280	997,9261	35,11313	26,31688	912,4353	309,442	5,288405	3,294897	32,90141

Alla inlopps- och utloppstemperaturer mättes, inklusive den varma sidans volymflöde. De resterande värdena är uträknade med hjälp av insamlade data.

Genom att utföra de ovannämnda experimenten och korrelera resultaten med ekvation (16), så kunde värden för parametrarna *C*, *m*, och *n* uppskattas för varje värmeväxlare som inkluderas i beräkningsprogrammet. Tabell 7.2 innehåller en jämförelse mellan två olika teoretiska modeller som använts och modellen som byggts upp baserat på experimentella data. Som inputdata används experiment som inkluderas i appendix A. Den första kolumnen i varje tabell beskriver vilket experiment i appendix A som används.

Tabell 7.2. Jämförelse av resultaten mellan olika beräkningsmodeller.

HP-52B	Svar	Martin Modell	Dovic et al Modell	Experimentell Modell
10 plattor				
2	10	6	0	6
3	10	6	0	6
4	10	6	0	4
5	10	6	0	6
6	10	6	0	6
30 plattor				
2	30	30	28	30
3	30	36	34	36
4	30	34	32	34
5	30	36	34	34
6	30	36	32	36
7	30	34	30	32
60 plattor				
2	60	38	34	38
3	60	46	44	48
4	60	48	48	52

HP-33	Svar	Martin Modell	Dovic et al Modell	Experimentell Modell
10 plattor				
3	10	10	0	8
4	10	10	0	8
5	10	10	0	8
6	10	10	0	8
7	10	6	0	6
30 plattor				
1	30	28	22	28
2	30	34	26	30
3	30	36	26	32
4	30	38	28	34
5	30	36	26	32
6	30	34	24	30
60 plattor				
1	60	40	34	42
2	60	54	46	56
3	60	60	50	60
4	60	46	44	52

HP-64	Svar	Martin Modell	Dovic et al Modell	Experimentell Modell
10 plattor				
2	10	8	0	6
3	10	10	0	6
4	10	8	0	6
5	10	10	0	8
6	10	10	0	8
30 plattor				
2	30	34	26	20
3	30	42	34	26
4	30	48	40	28
5	30	48	40	30
52 plattor				
1	52	92	82	54
2	52	104	86	62

Den teoretiska modellen baserad på Martins Nusselt ekvation (Sekulić och Shah, 2003, s. 515) visade sig ge relativt goda uppskattningar på värmeöverföringen, medan en annan teoretisk modell baserad på ekvationer från Dović et al. (Dović et al., 2009, s. 4553–4563) misslyckas med att ge uppskattningar för värmeväxlare med få plattor. Den experimentella modellens uppskattningar korrelerade bäst med testdata, speciellt för HP-64, vilket var den största värmeväxlaren som testades.

Ett separat testupplägg konstruerades för att mäta tryckfallet i värmeväxlarna. Data samlades in genom att låta volymflödet variera mellan ungefär 250 l/h och 2 000 l/h, och resultaten jämfördes med uppskattningar från ekvation (34). Den teoretiska modellen visade sig underskatta tryckfallet med 10–30 % för alla värmeväxlare. Figur 7.1 innehåller en jämförelse mellan olika teoretiska uppskattningar och tryckfallsdata för HP-52B med 30 stycken plattor. Den gula linjen i figuren är en korrigerad teoretisk uppskattning på tryckfallet vilket sammanfaller väldigt bra med uppmätta data. Separata korrektionsfaktorer konstruerades för alla värmeväxlare som inkluderades i modellen.

Figur 7.1. Experimentellt uppmätta tryckfall samt teoretiska uppskattningar för värmeväxlaren HP-52B med 30 stycken plattor.

7.3 Programvaruutveckling

Det bestämdes i ett tidigt skede att utvecklingen av ett fristående beräkningsprogram var nödvändigt för att bäst kunna uppfylla projektets mål. Programmet utvecklades med programmeringsspråket Python, biblioteket PyQt5 användes som grund för användargränssnittet, och programvarupaketet ReportLab användes för att generera beräkningsrapporter.

En bild på användargränssnittet för beräkningsprogrammet presenteras i figur 7.2. För att utföra en beräkning fyller användaren i fem av följande sju alternativ: $\dot{Q}$, $\dot{V}_{prim}$, $\dot{V}_{sek}$, $T_{prim,\,in}$, $T_{prim,\,ut}$, $T_{sek,\,in}$, $T_{sek,\,ut}$. Programmet beräknar de uteblivna värdena tillsammans med den uppskattade värmeytan. Dessutom kan användaren mata in frivilliga parametrar som en designmarginal samt ett maximalt tryckfall som inte får överstigas i värmeväxlaren. Programmet tillåter även användaren att välja mellan olika värmeväxlarmodeller, platt material, och anslutningstyper.

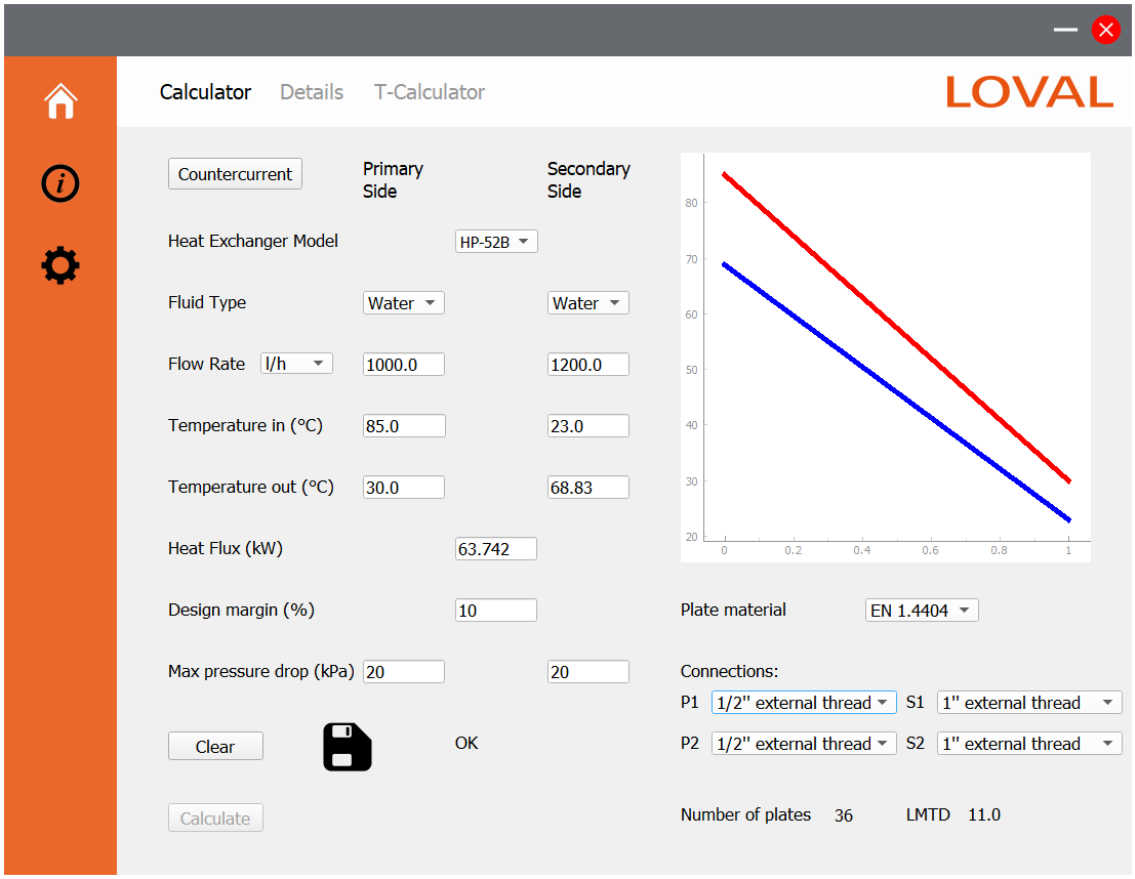

Figur 7.2. Beräkningsprogrammets användargränssnitt efter en beräkning.

En efterfrågad funktion var förmågan att generera rapporter på utförda beräkningar. Denna rapport konstrueras med programvarupaketet ReportLab när användaren trycker på ”spara ikonen”. En exempelrapport inkluderas i bilaga C. Användaren har även möjligheten att implementera nya värmeväxlare med godtyckliga dimensioner och designparametrar. Detta möjliggörs genom att modifiera en textfil som läses när programmet startas.

8 References

Alfa-Laval (n.d.) *How GPHEs works* [Online]. Available at https://test.alfalaval.com/fi/microsites/tiivisteelliset-levylammonvaihtimet/tyokalut/levylammonvaihtimen-toiminta/ (Accessed 23 June 2021).

Asif, M., Aftab, H., Syed, H. A., Ali, M. A. and Muizz, P. M. (2017) 'Simulation of corrugated plate heat exchanger for heat and flow analysis', International Journal of Heat and Technology, vol. 35, pp. 205–210.

Dović, D., Palm, B. and Švaić, S. (2009) 'Generalized correlations for predicting heat transfer and pressure drop in plate heat exchanger channels of arbitrary geometry', International Journal of Heat and Mass Transfer, vol. 52, no. 19, pp. 4553–4563.

Fernández-Seara, J., Uhía, F. J. and Sieres, J. (2007) 'Laboratory Practices with the Wilson Plot Method', Experimental Heat Transfer, vol. 20, no. 2, pp. 123–135.

Fernández-Seara, J., Uhía, F. J., Sieres, J. and Campo, A. (2007) 'A general review of the Wilson plot method and its modifications to determine convection coefficients in heat exchange devices', Applied Thermal Engineering, vol. 27, pp. 2745–2757.

Gherasim, I., Galanis, N. and Nguyen, C.T. (2011) 'Heat transfer and fluid flow in a plate heat exchanger. Part II: Assessment of laminar and two-equation turbulent models', International Journal of Thermal Sciences, Vol 50, pp. 1499–1511

Kays, W., Crawford, M. and Weigan, B. (2005) *Convective Heat and Mass Transfer*, 4th edn.

Martin, H. (1996) 'A theoretical approach to predict the performance of chevron-type plate heat exchangers', Chemical Engineering and Processing: Process Intensification, vol. 35, no. 4, pp. 301–310.

Opatřil, J., Jan, H., Ondřej, B. and Dlouhý, O. (2016) 'An experimental assessment of the plate heat exchanger characteristic by Wilson plot method', Acta Polytechnica, vol. 56, no. 5, pp. 367–372.

ReportLab-Inc (2021) *ReportLab Open Source* [Online]. Available at https://www.reportlab.com/opensource/ (Accessed 3 September 2021).

Rose, J. W. (2004) 'Heat-transfer coefficients, Wilson plots and accuracy of thermal measurements', Experimental Thermal and Fluid Science, vol. 28, pp. 77–86.

Sekulić, D. P. and Shah, R. K. (2003) *Fundamentals of Heat Exchanger Design*, New Jersey, John Wiley & Sons, Inc.

Shell-Oil-Company (2010) *Shell Tellus S2 V Technical Data Sheet* [Online]. Available at https://www.mil-specproducts.com/Documents/1463_tellus_s2_v32.pdf (Accessed 25 July 2021).

Sieder, E. N. and Tate, G. E. (1936) 'Heat Transfer and Pressure Drop of Liquids in Tubes', Industrial & Engineering Chemistry Research, vol. 28, pp. 1429–1435.

United-States-Geological-Survey (n.d.) *Water Density* [Online]. Available at https://www.usgs.gov/special-topic/water-science-school/science/water-density?qt-science_center_objects=0#qt-science_center_objects (Accessed 3 August 2021).

Wang, L., Sundén, B. and Manglik, R. M. (2007) *Plate Heat Exchangers*, Southampton, WIT Press.

Wójs, K. and Tietze, T. (1997) 'Effects of the temperature interference on the results obtained using the Wilson plot technique', Heat and Mass Transfer, vol. 33, pp. 241–245.

Zahid, A. (2003) 'Plate Heat Exchanger Literature Survey and New Heat Transfer and Pressure Drop Correlations for Refrigerant Evaporators', Heat Transfer Engineering, vol. 24, no. 5, pp. 3–16.

Zhu, X. and Haglind, F. (2020) 'Relationship between inclination angle and friction factor of chevron-type plate heat exchangers', International Journal of Heat and Mass Transfer, vol. 162.

Appendix A

Heat Transfer and pressure drop experiments performed with HP-33.

Exchanger model	HP-33
Number of plates	10

A_per_plates	0,03812		Hydr_diam	0,002749
A_cross	0,000189			

Experiment	T hot in	T hot out	T cold in	T cold out	V hot	V cold	T mean h	T mean c	Re hot	Re cold	LMTD	U	Heat Flux
#	°C	°C	°C	°C	l/h	l/h	°C	°C			°C	kW/m2K	kW
1	42,187	23,98467	22,862	28,417	266	869,8664	33,0858333	25,6395	356,0693	786,5726	5,04524	2,91547	5,607165
2	42,68579	23,28947	21,04684	29,30210526	375	879,3211	32,9876316	25,17447	501,9774	795,122	6,236642	3,543084	8,423355
3	43,067	23,656	18,94	31,215	540	852,2129	33,3615	25,0775	722,8475	770,6095	7,743596	4,112261	12,13881
4	43,33344	24,95656	16,86938	33,0103125	752	854,454	34,145	24,93984	1006,632	772,636	9,159718	4,583414	16,00384
5	43,46333	26,23233	14,407	34,147	1010	879,8581	34,8478333	24,277	1351,993	795,6075	10,52102	5,025228	20,15424
6	43,39967	27,516	11,52433	35,46266667	1235	817,8087	35,4578333	23,4935	1653,179	739,4997	11,49792	5,182986	22,71707
7	43,37579	36,97737	32,12368	39,52947368	1235	1064,869	40,1765789	35,82658	1653,179	962,9031	4,33049	5,543506	9,151123

Exchanger model	HP-33
Number of plates	30

Experiment	T hot in	T hot out	T cold in	T cold out	V hot	V cold	T mean h	T mean c	Re hot	Re cold	LMTD	U	Heat Flux
#	°C	°C	°C	°C	l/h	l/h	°C	°C			°C	kW/m2K	kW
1	43,07529	22,16412	20,32147	31,24558824	535	1022,054	32,6197059	25,78353	205,1627	308,0625	5,371088	2,109261	12,95588
2	43,20697	21,38424	17,26758	32,98363636	760	1053,19	32,2956061	25,12561	291,446	317,4475	6,71336	2,501745	19,2069
3	43,22649	23,32811	14,36514	36,34432432	1127	1018,258	33,2772973	25,35473	432,1838	306,9184	7,876814	2,883045	25,97025
4	42,74514	25,314	11,696	37,82485714	1510	1005,334	34,0295714	24,76043	579,0572	303,0228	8,543707	3,119729	30,48158
5	42,42212	28,8003	11,22121	39,32212121	1980	957,8728	35,6112121	25,27167	759,2936	288,7173	8,343816	3,273377	31,23452
6	40,15594	29,84969	12,31844	37,9128125	2348	943,5875	35,0028125	25,11563	900,4148	284,4115	7,435442	3,295736	28,02421

Exchanger model	HP-33
Number of plates	60

Experiment	T hot in	T hot out	T cold in	T cold out	V hot	V cold	T mean h	T mean c	Re hot	Re cold	LMTD	U	Heat Flux
#	°C	°C	°C	°C	l/h	l/h	°C	°C			°C	kW/m2K	kW
1	43,02938	22,42344	20,93844	31,5103125	635	1235,213	32,7264063	26,22438	119,9626	198,8942	4,898037	1,352616	15,15307
2	43,0081	21,50929	18,18762	33,695	912	1261,824	32,2586905	25,94131	172,2928	203,179	5,811534	1,70824	22,70617
3	42,512	23,546	14,57667	37,46366667	1405	1161,96	33,029	26,02017	265,4291	187,0989	6,822059	1,97773	30,85934
4	42,35563	27,04156	13,1225	39,3384375	1800	1049,362	34,6985938	26,23047	340,0515	168,9684	7,130376	1,957406	31,92255

HP-33 Target flowrate (l/h)	250	500	750	1000	1250	1500	1750	2000	2250	2500	2750
10pl											
flow (l/h)	249,6	498,483	749,339	999,664	1249,43						
pressure drop (kpa)	2,1792	7,77467	16,3014	27,3166	40,652						
30pl											
flow (l/h)	249,795	499,939	749,724	999,767	1249,89	1499,88	1749,88	1999,76	2248,51	2401,33	
pressure drop (kpa)	0,34347	1,09388	2,35483	4,00897	5,97417	8,28095	10,9258	13,905	17,255	19,4367	
60pl											
flow (l/h)	250,469	499,927	750,125	999,978	1249,84	1499,78	1749,86	1999,64	2250,16	2499,84	2653,76
pressure drop (kpa)	0,14333	0,38375	0,77625	1,30826	1,95458	2,73417	3,62087	4,62708	5,74625	6,97083	7,76217

Heat Transfer and pressure drop experiments performed with HP-52B.

Exchanger model	HP-52B
Number of plates	10

A_per_plates	0,06294		Hydr_diam	0,00286
A_cross	0,000189			

Experiment	T hot in	T hot out	T cold in	T cold out	V hot	V cold	T mean h	T mean c	Re hot	Re cold	LMTD	U	Heat Flux
#	°C	°C	°C	°C	l/h	l/h	°C	°C			°C	kW/m2K	kW
1	45,34727	20,40091	19,1591	29,58	350	836,1758	32,874091	24,369545	489,25	777,857	5,71562	2,81073	10,11137
2	45,41809	19,35085	16,8972	31,14489362	460	839,9186	32,384468	24,021064	643,015	781,339	6,71254	3,2868	13,88633
3	44,90311	20,31467	17,0978	32,62977778	540	853,1499	32,608889	24,863778	754,844	793,647	6,76352	3,6121	15,37657
4	45,36769	19,44092	14,9366	33,11046154	600	854,2416	32,404308	24,023538	838,715	794,663	7,74454	3,69583	18,015
5	44,96575	21,78875	13,4053	36,26125	798	807,5842	33,37725	24,83325	1115,49	751,259	8,54299	3,98344	21,41878
6	45,69759	22,71944	13,428	37,19740741	894	862,5046	34,208519	25,312685	1249,69	802,349	8,88996	4,25168	23,7896

Exchanger model	HP-52B
Number of plates	30

Experiment	T hot in	T hot out	T cold in	T cold out	V hot	V cold	T mean h	T mean c	Re hot	Re cold	LMTD	U	Heat Flux
#	°C	°C	°C	°C	l/h	l/h	°C	°C			°C	kW/m2K	kW
1	44,87	21,78111	21,1344	30,11444444	420	1077,458	33,325556	25,624444	168,08	334,104	4,51117	1,31809	11,22751
2	45,05417	19	17,085	34,87333333	720	1052,201	32,027083	25,979167	288,137	326,272	4,94726	2,32503	21,71904
3	44,96111	18,86056	13,055	38,80888889	1038	1049,611	31,910833	25,931944	415,398	325,469	5,97721	2,77927	31,36737
4	44,90368	22,44632	11,6705	41,65894737	1350	1008,703	33,675	26,664737	540,258	312,784	6,27448	2,96277	35,10133
5	43,71056	24,42611	11,6733	41,40722222	1600	1035,38	34,068333	26,540278	640,306	321,056	6,10582	3,09861	35,72383
6	42,92231	26,88231	11,8746	41,49153846	1910	1032,101	34,902308	26,683077	764,365	320,039	5,77655	3,25201	35,47061
7	41,345	28,88125	12,1106	40,523125	2280	997,9261	35,113125	26,316875	912,435	309,442	5,28841	3,2949	32,90141

Exchanger model	HP-52B
Number of plates	60

Experiment	T hot in	T hot out	T cold in	T cold out	V hot	V cold	T mean h	T mean c	Re hot	Re cold	LMTD	U	Heat Flux
#	°C	°C	°C	°C	l/h	l/h	°C	°C			°C	kW/m2K	kW
1	42,73565	23,92348	22,4826	33,66782609	690	1159,331	33,329565	28,075217	135,76	194,224	4,14624	0,96004	15,0322
2	43,6095	22,88575	19,0578	38,30725	1060	1140,036	33,247625	28,6825	208,559	190,991	4,52517	1,48866	25,43951
3	43,95804	23,45435	14,5528	41,19826087	1467	1127,725	33,706196	27,875543	288,638	188,929	5,24455	1,75878	34,83348
4	42,69489	29,74289	11,8516	42,20555556	2370	1010,26	36,218889	27,028556	466,306	169,25	4,83519	1,94683	35,54838

HP-52B Target flowrate (l/h)	250	500	750	1000	1250	1500	1750	2000	2250	2500	2750
10pl											
flow (l/h)	249,5625	498,9479	749,5125	999,2895	1247,929						
pressure drop (kpa)	3,42291667	12,08792	25,4935	43,45368	65,74714						
30pl											
flow (l/h)	250,130435	499,8958	749,9348	1000,094	1249,708	1500,087	1749,844	2000,185	2249,656		
pressure drop (kpa)	0,5726087	1,866667	3,903913	6,4984	9,891667	13,79522	18,19708	23,12391	28,535		
60pl											
flow (l/h)	249,913043	499,8958	749,9688	999,8152	1250,385	1499,792	1749,946	1999,917	2249,511	2498,802	2572,938
pressure drop (kpa)	0,2226087	0,621667	1,2575	2,106522	3,131667	4,345833	5,74	7,299583	9,03913	10,93625	11,52917

Heat Transfer and pressure drop experiments performed with HP-64.

Exchanger model	HP-64
Number of plates	10

A_per_plates	0,072207		Hydr_diam	0,003336
A_cross	0,000252			

Experiment	T hot in	T hot out	T cold in	T cold out	V hot	V cold	T mean h	T mean c	Re hot	Re cold	LMTD	U	Heat Flux
#	°C	°C	°C	°C	l/h	l/h	°C	°C			°C	kW/m2K	kW
1	40,908	24,58886	23,78629	29,61714286	344	960,8405	32,7484286	26,701714	416,2198	818,2694	3,966934	2,269636	6,501153
2	40,94823529	23,25412	21,99853	30,41029412	450	944,6746	32,1011765	26,204412	544,4736	804,5022	4,363283	2,926734	9,220958
3	41,15297297	23,69595	21,44514	32,06432432	595	976,1663	32,4244595	26,75473	719,9151	831,3211	4,899092	3,400376	12,02879
4	41,1675	23,32556	19,43222	33,10944444	742	965,9977	32,2465278	26,270833	897,7764	822,6614	5,725439	3,708451	15,33136
5	41,33575758	24,32727	18,04848	34,73757576	966	982,5123	32,8315152	26,39303	1168,803	836,7255	6,437164	4,093582	19,02731
6	41,388125	26,00313	17,4675	36,115625	1190	979,7995	33,695625	26,791563	1439,83	834,4152	6,773567	4,334932	21,20211

Exchanger model	HP-64
Number of plates	30

Experiment	T hot in	T hot out	T cold in	T cold out	V hot	V cold	T mean h	T mean c	Re hot	Re cold	LMTD	U	Heat Flux
#	°C	°C	°C	°C	l/h	l/h	°C	°C			°C	kW/m2K	kW
1	41,72366667	22,894	22,265	30,81966667	436	957,7539	32,3088333	26,542333	152,3361	271,8803	3,601783	1,218556	9,507443
2	41,90484848	21,90606	19,8403	35,01636364	694	912,7083	31,9054545	27,428333	242,48	259,093	4,00441	1,852929	16,07303
3	41,98261905	22,80857	18,195	37,81047619	1000	975,535	32,3955952	28,002738	349,3948	276,9278	4,389158	2,335429	22,20488
4	41,99709677	22,55871	12,91161	39,48741935	1346	982,5321	32,2779032	26,199516	470,2854	278,9141	5,300709	2,638793	30,29981
5	41,85645161	25,11516	11,46097	40,46258065	1705	982,2433	33,4858065	25,961774	595,7181	278,8321	5,372711	2,840232	33,05582
6 Low LMTD	41,61266667	23,53267	21,76233	34,52266667	958	1354,659	32,5726667	28,1425	334,7202	384,5507	3,833946	2,415194	20,0585
7 Co-Currnet	34,09193548	22,84323	13,71065	21,24612903	740	1101,66	28,4675806	17,478387	232,4026	252,0755	10,88383	0,409282	9,649511

Exchanger model	HP-64
Number of plates	60

Experiment	T hot in	T hot out	T cold in	T cold out	V hot	V cold	T mean h	T mean c	Re hot	Re cold	LMTD	U	Heat Flux
#	°C	°C	°C	°C	l/h	l/h	°C	°C			°C	kW/m2K	kW
1	42,40666667	26,96444	22,6237	31,04888889	540	987,7613	34,6855556	26,836296	92,94753	144,9119	7,295296	0,305538	9,656909
2	43,15135135	26,29946	13,19216	40,06	1660	1039,087	34,7254054	26,626081	285,7276	152,4417	6,933558	1,078462	32,396
3	42,86612903	28,39484	11,97484	41,08580645	2135	1059,196	35,6304839	26,530323	367,487	155,3919	6,589387	1,253326	35,77995
4	43,46589286	24,79321	18,81643	36,15410714	1055	1133,956	34,1295536	27,485268	181,5919	166,3596	6,621872	0,795211	22,81359
5	43,33545455	22,97939	13,39121	38,79666667	1456	1164,276	33,1574242	26,093939	250,6141	170,8079	6,751688	1,173402	34,32335

HP-64 Target flowrate (l/h)	250	500	750	1000	1250	1500	1750	2000	2250	2500	2750
10pl											
flow (l/h)	250,075	499,25	749,7813	1000	1249,688	1482,631					
pressure drop (kpa)	2,1925	7,895789	16,63438	28,23882	42,62563	58,43381					
30pl											
flow (l/h)	250,4479	500,1739	750,1771	999,6667	1249,469	1499,906	1749,615	1999,719	2250,181	2443,971	
pressure drop (kpa)	0,33625	1,086522	2,325	3,980417	5,981667	8,32	10,98375	13,985	17,27206	20,02176	
60pl											
flow (l/h)	250,3958	499,9583	749,8854	999,8043	1250	1500,26	1750,185	1999,542	2249,587	2499,417	2646,264
pressure drop (kpa)	0,135417	0,357083	0,711667	1,183913	1,775	2,489583	3,323478	4,27625	5,340435	6,516667	7,222222

Appendix B

MATLAB script for performing the modified Wilson plot method. This specific code uses data from the 30-plate version of the HP-33 heat exchanger.

```
clc
clear all
format shortG

%Read in data from an excel file
filename = 'Data_insamling_HP33.xlsx';
sheet = 2;

%Heat exchanger and fluid characteristics
Dh = 0.002749;
A_per_plate = 0.03812;
n_plates = 30;
Tot_area = A_per_plate*n_plates;
therm_cond_hot = 0.619;
Pr_hot = 4.95;

%Ininital m and n guess
m_guess = 0.6;
n_guess = 0.333;

%Data = [Th_in, Th_out, Tc_in, Tc_out, Vw_flow, Vc_flow, Re_w, Pr_w,
Re_c, Pr_c, Q_tot, U_tot, R_tot, LMTD]
Data1 = xlsread(filename,sheet,'G15:T20');

Re_hot = Data1(:,7);
R_tot = Data1(:,13);
Y = R_tot;

iterations = 0;

%Loops until a satisfactory m value has been found
while true

    %Performs Wilson plot as described in 4.8.1
    X = 1./(Re_hot.^m_guess);
    parameters = polyfit(X,Y,1);
    C1 = parameters(2);
    C2 = parameters(1);

    %Performs Modified Wilson plot as described in 4.8.2
    Y2 = log(1./(R_tot-C1));
    X2 = log(Re_hot);

    parameters2 = polyfit(X2,Y2,1);
    m_guess_save = m_guess;

    %If the slope of the line described by parameters2 is equal to
m_guess,
    %break, otherwise make a new guess
```

```
    if (m_guess*1.001 >= parameters2(1)) && (m_guess*0.999 <=
parameters2(1))
        break
    end

    if m_guess > parameters2(1)
        m_guess = m_guess + (m_guess - parameters2(1));
    end

    if m_guess < parameters2(1)
        m_guess = m_guess - (parameters2(1) - m_guess);
    end
    iterations = iterations + 1;
end

%Calculates and prints out the relevant parameters
iterations
m = m_guess_save
C = 1/(C2*(therm_cond_hot/Dh)*Pr_hot.^(n_guess)*Tot_area)
C1 = parameters(2)
C2 = parameters(1)


%Draws Figure 2.8
f1 = figure;
fh=@(x) parameters(1).*x+parameters(2);
x_lim_max = (1/(Re_hot(1).^m))*1.2;
y_lim_max = max(R_tot)*1.2;
x_val = 0:x_lim_max/100:x_lim_max;

hold on
graph1 = plot(X,Y,'*');
graph2 = plot(x_val,fh(x_val),'r');
xlim([0 x_lim_max])
ylim([0 y_lim_max])
xlabel('1/Re^n')
ylabel('R tot')
hold off


%Draws Figure 2.9
f2 = figure;
gh=@(x) parameters2(1).*x+parameters2(2);
x_lim_max = max(log(Re_hot))*1.2;
y_lim_max = max(log(1./(R_tot-C1)))*1.2;
x_val = 0:x_lim_max/100:x_lim_max;

hold on
graph3 = plot(X2,Y2,'*');
graph4 = plot(x_val,gh(x_val),'r');
xlim([0 x_lim_max])
ylim([-4 y_lim_max])
xlabel('ln(Re)')
ylabel('ln(1/(Re tot-C1))')
hold off
```

Appendix C

Two-page A4 example report generated after a calculation has been performed

LOVAL

Calculation summary

Date: 22.11.2021

Design Parameters

	Primary Side		Secondary Side
Fluid composition	**Water**		**Water**
Inlet temperature (°C)	**85.0**		**22.0**
Outlet temperature (°C)	**30.0**		**67.83**
Heat load (kW)		**63.7**	
LMTD (°C)		**12.0**	
Thermal length	**4.6**		**3.8**
Fluid flow rate (l/h)	**1000.0**		**1200.0**

Heat Exchanger Parameters

	Primary Side		Secondary Side
Heat Exchanger Model		**HP-52B**	
Heat transfer area (m2)		**1.76**	
Number of plates		**28**	
Number of passages	**13**		**14**
Channel volume (l)	**1.17**		**1.26**

Fluid Parameters

	Primary Side		Secondary Side
Refrence temperature (°C)	**57.5**		**44.91**
Density (kg/m3)	**984.6**		**990.4**
Dynamic viscosity (cP)	**0.49**		**0.6**
Thermal conductivity (W/mK)	**0.65**		**0.63**
Prandtl Number	**3.15**		**3.95**

Flow Parameters

	Primary Side		Secondary Side
Overfall Heat Transfer Coefficient (W/m2K)		**3300**	
Pressure drop total (kPa)	**8.04**		**10.98**
Pressure drop core (kPa)	**7.73**		**9.57**
Pressure drop fitting (kPa)	**0.31**		**1.41**
Reynold Number	**630**		**573**
Fluid velocity (m/s)	**0.114**		**0.127**

LOVAL

Calculation summary

Date: 22.11.2021

Brazed Plate Heat Exchanger - HP-52B

Plates	Length	Primary volume	Secondary volume	Heat transfer area	Weight	Design margin
28	68	1.17	1.26	1.76	7.4	10
pcs	mm	liters	liters	m2	kg	%

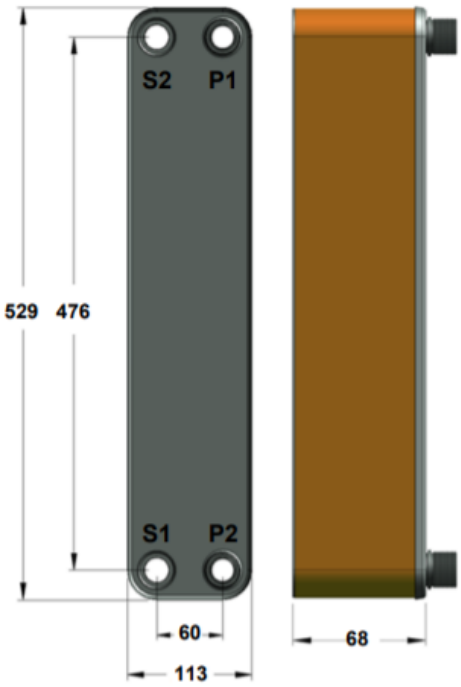

Connection	Type	Position
P1 - Primary inlet	1" external thread	Front
P2 - Primary outlet	1" external thread	Front
S1 - Secondary inlet	3/4" external thread	Front
S2 - Secondary outlet	3/4" external thread	Front

Materials	
HEX plates	EN 1.4404
End plates	EN 1.4301
Connections	EN 1.4301
Brazing material	Pure copper

Operating conditions	
Temperature	-196/150 °C
Primary side pressure	-1/32 bar
Secondary side pressure	-1/32 bar